Geochemistry, Geophysics, and Geosystems (G3)
FEB 28 2007; 8 NIL_62-NIL_87
http://dx.doi.org/10.1029/2006GC001400

An edited version of this paper was published by AGU.

Geochemical fluxes related to alteration of a subaerially exposed seamount: Nintoku seamount, ODP Leg 197, Site 1205

Sidonie Révillon[*1], Damon A.H. Teagle[1], Philippe Boulvais[2], John Shafer[3], and Clive R. Neal[3]

1 National Oceanography Centre, School of Ocean and Earth Science, University of Southampton, European Way, Southampton SO14 3ZH, United Kingdom
2 Géosciences Rennes, UMR 6118, Université de Rennes 1, Campus de Beaulieu, 35042, Rennes Cedex, France
3 Department of Civil Engineering and Geological Sciences, University of Notre Dame, 156 Fitzpatrick Hall, Notre Dame IN 46556, USA

* Corresponding author : Present affiliations : Ifremer, département de Géosciences Marines, BP70, 29280, Plouzané, France and UMR6538 "Domaines Océaniques", Institut Universitaire Européen de la Mer, Place Nicolas Copernic, 29280 Plouzané, France: Sidonie.revillon@ifremer.fr

Abstract:

Hole 1205A was drilled on Nintoku Seamount, which lies in the midportion of the Emperor Seamount Chain. This seamount was emergent ~56 Myr ago but was submerged by 54 Ma, so the lavas have endured weathering in both subaerial and submarine environments. We have studied the petrology, mineralogy, and geochemistry of intercalated altered basalts, breccias, and soil samples recovered at Hole 1205A to quantify the chemical exchanges between the seamount and seawater and/or meteoric fluids. The secondary mineralogy is relatively uniform throughout the section and comprises smectite, Fe-oxyhydroxides, iddingsite, and Ca-carbonates. Soils are composed of variably altered basaltic clasts in a matrix of kaolinite, smectite, and vermiculite with minor goethite, hematite, and magnetite. Throughout the basement section, altered basalts, breccias, and soils are depleted in Si, Mg, Ca, Na, Sr, Rb, and Ba and enriched in Fe. Fe^{3+}/Fe_T (up to ~1), $\delta^{18}O$ (up to ~+20‰), and $^{87}Sr/^{86}Sr$ ratios are strongly elevated relative to primary igneous values. Differences in the $^{87}Sr/^{86}Sr$ ratios define an Upper Alteration Zone with $^{87}Sr/^{86}Sr$ close to 56 Ma seawater (~0.7077) from a Lower Alteration Zone where $^{87}Sr/^{86}Sr$ are less elevated (~0.704). The Lower Alteration Zone likely reflects interaction with a subaerial oxidizing fluid at low temperature. This zone probably retained most of the original subaerial weathering signature. The Upper Alteration Zone was altered through circulation of large quantities of cold oxidizing seawater that partially overprinted the subaerial weathering chemical characteristics. Altered samples were compared to estimated protolith compositions to calculate chemical gains and losses. Global chemical fluxes are calculated for the entire basement section using different lithological proportions models and different rates of oceanic island emplacement. Although the global construction rate of ocean islands is small compared to igneous accretion at mid-ocean ridges, the magnitude of the chemical changes indicates that ocean islands and seamounts may be a significant contributor to the chemical budget of the oceans.

Abstract:

Hole 1205A was drilled on Nintoku Seamount, which lies in the mid-portion of the Emperor Seamount Chain. This seamount was emergent ~56 Ma ago but was submerged by 54 Ma, so the lavas have endured weathering in both subaerial and submarine environments. We have studied the petrology, mineralogy and geochemistry of intercalated altered basalts, breccias and soil samples recovered at Hole 1205A to quantify the chemical exchanges between the seamount and seawater and/or meteoric fluids. The secondary mineralogy is relatively uniform throughout the section and comprises smectite, Fe-oxyhydroxides, iddingsite and Ca-carbonates. Soils are composed of variably altered basaltic clasts in a matrix of kaolinite, smectite and vermiculite with minor goethite, hematite and magnetite. Throughout the basement section, altered basalts, breccias and soils are depleted in Si, Mg, Ca, Na, Sr, Rb and Ba and enriched in Fe. Fe^{3+}/Fe_T (up to ~1), $\delta^{18}O$ (up to ~+20‰) and $^{87}Sr/^{86}Sr$ ratios are strongly elevated relative to primary igneous values. Differences in the $^{87}Sr/^{86}Sr$ ratios define an Upper Alteration Zone with $^{87}Sr/^{86}Sr$ close to 56 Ma seawater (~0.7077) from a Lower Alteration Zone where $^{87}Sr/^{86}Sr$ are less elevated (~0.704). The Lower Alteration Zone likely reflects interaction with a subaerial oxidizing fluid at low temperature. This zone probably retained most of the original subaerial weathering signature. The Upper Alteration Zone was altered through circulation of large quantities of cold oxidizing seawater that partially overprinted the subaerial weathering chemical characteristics. Altered samples were compared to estimated protolith compositions to calculate chemical gains and losses. Global chemical fluxes are calculated for the entire basement section using different lithological proportions models and different rates of oceanic island emplacement. Although the global construction rate of ocean islands is small compared to igneous accretion at mid-ocean ridges, the magnitude of the chemical changes indicate that ocean islands and seamounts may be a significant contributor to the chemical budget of the oceans.

Keywords:

Ocean Drilling Program, Hole 1205A, Alteration, Chemical fluxes, isotope geochemistry, Oceanic Island.

1. Introduction:

Circulation of fluid through the oceanic basement is the main mechanism of heat and chemical elements transfers between the lithosphere and the oceans. These processes are a major regulator of the chemical and isotopic composition of seawater. There have been extensive studies of fluid circulation at mid ocean ridge spreading centres and the geometry and chemical characteristics of high temperature hydrothermal systems are well understood (e.g., Alt, 1995; 2003a). Recently, considerable efforts have been made to account for low temperature and ridge flank fluid circulation system influence on the geochemistry of the oceanic crust and seawater (Alt, 2003a; Alt et al., 1996; Alt and Teagle, 1999; Staudigel et al., 1996; Schramm et al., 2005).

Although such studies have led to a greater understanding of hydrothermal processes, the fluid and chemical fluxes remain poorly constrained. A common approach has been to balance known continental inputs (e.g., rivers and groundwater flows) and outputs (e.g., from hydrothermal, ridge flank or back arc circulations) from the seawater reservoir (e.g., Elderfield and Schultz, 1996; Palmer and Edmond, 1989). However, for such approaches to be successful it is imperative that the global riverine budget is accurate and that there are no significant unaccounted for sources or sinks in the global chemical cycle (Davis et al., 2003). To date, contributions from other oceanic features such as oceanic islands have rarely been taken into account when calculating seawater elemental budgets (Bach et al., 2003; Davis et al., 2003; Elderfield and Schultz, 1996; Mottl and Wheat, 1994; Teagle et al., 2003). However, given the large number of oceanic islands and seamounts on the

ocean floor, and their potential propensity to weather rapidly, the assumption that these features have no influence on global chemical budgets requires investigation.

In this paper, we have studied samples from Nintoku seamount on the Emperor Seamount Chain that were collected during ODP (Ocean Drilling Program) Leg 197. We focused on the characterisation of the alteration conditions and in quantifying chemical fluxes provided to the oceans through interactions with seawater and subaerial fluids. We are interested in establishing preliminary effects of seamount and oceanic island basalt alteration to demonstrate whether ocean islands can plausibly be significant contributors to global geochemical cycles.

2. Geological background: ODP Leg 197, the Emperor Seamount Chain and Nintoku Seamount:

Nintoku Seamount occupies a central position in the Emperor Seamount Chain (Figure 1). It is an elongated volcanic edifice formed by the coalescence of multiple eruptive centres, much like many of the larger seamounts in this chain (Shipboard Scientific Party, 2002). Site 1205, drilled during ODP Leg 197, is located at 41°19.998'N and 170°22.699'E in 1310 m of water on the north western edge of Nintoku seamount approximately 100 m southwest of DSDP Site 432. Seismic reflection survey data (Dalrymple et al., 1981) and core material recovered by drilling at Site 432 indicate that Nintoku Seamount was in an intermediate atoll stage before subsidence removed the island below the wave base (Jackson et al., 1980). Nintoku Seamount apparently remained at or above sea level long enough to be almost completely flattened by subaerial erosion and wave action. ^{40}Ar-^{39}Ar measurements date the age of the seamount to be 55.6 ± 0.2 Ma (Duncan and Keller, 2004) and shipboard biostratigraphy studies gave an Eocene age in Zone NP10 to the sediment overlying the basement (presence of *T. contortus* nannofossils) with an estimated age range of 53.6-54.7 Ma (Shipboard Scientific Party, 2002).

Hole 1205A, with a total depth of 326 meters below seafloor (mbsf), penetrated 42.7 m of sediment with low recovery (2 to 16%) before reaching basement (Shipboard Scientific Party, 2002). The five sediment cores consist of sandstone and siltstone containing well-rounded to sub-rounded basalt clasts, volcanic ash, and fossil fragments of molluscs, benthic foraminifers, bryozoans, and coralline red algae indicating a relatively shallow-water, high-energy depositional environment (Shipboard Scientific Party, 2002). 283.2 m of basement were cored with a high recovery for volcanic rocks (56.5%).

3. Basement stratigraphy

Basement rocks in Hole 1205A have been divided into 30 lithologic units, of which 25 are lava flows (Figure 2). The lava flow units include a'a and pahoehoe, as well as transitional flow types ranging in thickness between 0.6 and 17 m, 3.7 and 24.9 m and 3.1 and 32.9 m respectively (Shipboard Scientific Party, 2002). Some lava flows are capped by red soil or deeply weathered flow tops. Many of the flows are highly vesicular (up to 50%), with 1- to 10-mm-diameter vesicles, especially close to unit boundaries. Several units contain auto-breccia horizons, which were formed during emplacement of the flow and which may occur either at the base of the unit (e.g., Units 8, 19, 24, 26, and 28), at the top of the unit (Units 3 and 30), or both (Unit 29). Most soil horizons and breccias were considered to be subunits of the underlying flow. The thickness and vesicularity of the flows from Site 1205, the presence of oxidized flow tops and soil horizons, together with the lack of pillow structure indicate that the flows erupted subaerially (Shipboard Scientific Party, 2002).

Lava flows range from aphyric to highly plagioclase and olivine-phyric basalt. Shipboard and shore-based geochemical analyses show that only one of the lava flow units (Unit 19B [245.1 to 254.5 mbsf]) has a tholeiitic composition, whereas all other units are alkali basalts (Shafer et al., 2005).

4. Analytical techniques:

All samples were prepared for analysis at the Southampton (now National) Oceanography Centre (SOC). Samples were carefully cut avoiding veins before repeated washing in distilled water and being ground to a fine powder in a WC shatterbox. X-ray diffraction analyses were performed on soil samples at SOC on oriented air-dried fractions. The same powders were scanned after saturation in ethylene-glycol, and then after heating to 490°C. Major and some trace elements were measured at the Université de Bretagne Occidentale, Brest, France by ICP-AES with an ISA Jobin-Yvon JY70 Plus apparatus (Cotten et al., 1995). Carbon and Sulfur concentrations were determined at the University of Leicester using a CS-125 LECO Carbon and Sulphur Determinator by high temperature combustion. The lower limit of detection are typically 12 ppm for C and 10 ppm for S. Ferrous iron concentrations were measured by $KMnO_4$ titration after reaction of the samples in $HF+H_2SO_4$ at SOC. Samples were dissolved in a hot mixture of 3:1 24 N HF and 12 N HNO_3. Trace element were analysed at SOC by ICP-MS on a VG Elemental PlasmaQuad PQ^{2+} in solution mode. $^{18}O/^{16}O$ and $^{13}C/^{12}C$ of separated carbonate samples were determined at SOC on a GEO 20-20 using a Carbonate Automatic Preparation System (CAPS). $^{87}Sr/^{86}Sr$ ratios of the samples were measured at SOC on VG Sector 54 TIMS in a multi-dynamic mode. NBS 987 gave $^{87}Sr/^{86}Sr$ =0.710250±15 (2σ, n = 12) during the time the Site 1205 samples were analyzed. For oxygen isotopic measurements, bulk rocks powders were reacted using BrF_5 following the method of Clayton and Mayeda, (1963). Isotopic analyses were performed on CO_2 using a VG SIRA 10 triple-collector mass spectrometer at the Université de Rennes. Isotopic compositions are quoted using the δ notation with respect to SMOW. During the course of analyses, repeated measurments of quartz international standard NSB28 and MORB glass material internal reference CIRCE 93 gave $\delta^{18}O$ = 9.42± 0.11 (1σ, n = 7) and $\delta^{18}O$ = 5.48 ± 0.11 (1σ, n = 9), respectively. Analyses were normalized to NBS 28 ($\delta^{18}O$= +9.60‰) and basaltic MORB Circe 93 (recommended value $\delta^{18}O$=+5.68‰). All O isotope analyses were repeated two or more times and the reproducibility is better than 0.2‰.

5. Alteration petrology and mineralogy:

5.1. Lava flows

The extent of alteration was determined petrographically from the proportion of secondary minerals and samples were classified into six broad categories. They are graded on a scale from 0 to 5 as follow: 0 = unaltered (<2%), 1 = slightly altered (2%-5%), 2 = moderately altered (5%-10%), 3 = highly altered (10%-15%), 4 = very highly altered (15%-20%), 5 = intensely altered (>20%) (see also Table 1 and Figure 2). The extent of alteration varies greatly withing the hole but there is no strong trend with depth. The alteration assemblage is homogeneous downhole and mainly comprises Fe-oxyhydroxides, iddingsite, Ca-carbonates, clay minerals (smectite) and minor zeolites. In thin section, Fe-oxyhydroxide, carbonate, and clay minerals partially to completely replace olivine phenocrysts, and plagioclase is partially altered to clay minerals (may be including some sericite) along cracks in the crystal structure. Vesicles are variably empty, lined or filled with secondary minerals. Vesicle fillings are homogeneous downhole being composed principally of Ca-Carbonate, clay minerals including smectite, zeolite (phillipsite), and Fe-oxyhydroxide (Figure 2). Veins are sparse (<<1% vol. of core), usually very thin (~0.5 mm wide) and do not present a preferred orientation. Veins are filled with variable proportions of clay minerals, Fe oxyhydroxide, carbonate and zeolite minerals.

5.2. Soils and Breccias

Recovered soil intervals are up to 30 cm thick although recovery of these loosely consolidated deposits is likely to be much lower than for the volcanic rocks (Barr et al., 2002; Brewer et al., 1998). Soils units, which represent substantial time intervals, were likely significantly thicker as also revealed by an increase in the drilling rates in intervals where soils were recovered. But, the absence of wireline logging data for Site 1205 precludes any estimates of their original thickness. Soils are present throughout the basement sequence (Figure 2). They are red brown, most commonly without structure but may be poorly bedded and containing round, highly altered basaltic clasts. The matrix is composed of opaque minerals, rare organic material, amorphous Fe-

oxyhydroxide, feldspar, palagonite and clays, together with basaltic lava fragments in various stages of alteration. X-Ray diffractograms of bulk soil samples and separated clay minerals identified kaolinite, smectite and vermiculite as the main clay phases, associated with goethite, hematite and magnetite (Figure 3). Remnant plagioclase and minor calcite are also present.

Breccias are generally poorly sorted, clast-supported, and are composed of angular clasts of the associated lava unit cemented by carbonate, clay, zeolite, and/or Fe-oxyhydroxides. Clasts vary in size from ~2 to >50mm. Breccia intervals are either interpreted as weathered flow tops or basal breccias.

6 Protolith compositions

To identify and quantify chemical changes during fluid-rock interactions, bulk rock compositions of altered samples are compared to the composition of a fresh precursor (protolith). Determination of an appropriate protolith composition for a suite of sample is essential to accurately establish elemental mobility and chemical fluxes (Laverne et al., 2001). We first examined the original geochemical heterogeneity downhole using trace element ratios, such as La/Yb (Table 1, Figure 4), which should be relatively insensitive to alteration or which alteration-induced variations are insignificant compared to magmatic-related variations (Ludden, 1978). Following Shafer et al. (2005), we distinguished three main series: an Upper Igneous Series composed of alkali basalts and their associated breccia and soil horizons, from Unit 1 to 18B (42.7 to 245.1 mbsf); a Tholeiitic Unit comprising Subunits 19A, B and C (245.1 to 254.5 mbsf); and a Lower Igneous Series composed of alkali basalts and associated breccia and soil horizons from Unit 20 to 30B (254.5 to 326 mbsf) (Figures 2 and 4). We also distinguished a High La/Yb and a Low La/Yb group in both alkali basalts Series. In the Upper Igneous Series, the former includes Units 6 to 11, and 17 and 18 and the latter Units 5 and 12 to 16 (Figure 4). Units 1 and 3B basalts have higher La/Yb ratios than the rest of the Series and probably derived from a more trace element-enriched mantle source (Figure 4). As we do not have samples of altered basalts, soils or breccias associated with these Units, they were not included in the following protolith composition calculations. In the Lower Igneous Series, the High La/Yb group is composed of Units 20 to 22 and the Low La/Yb group by Units 24 to 30.

In situ fractional crystallisation of some minerals, such as plagioclase or clinopyroxene, modifies the chemical composition of igneous rocks, and these changes must be identified to avoid false attribution to alteration processes. In the Upper Igneous Series, recovered basalt samples with LOI<4% have similar MgO contents (5.6-7 wt.%, data available in Shafer et al., 2005; Figure 5) and Nd contents between 15 and 22 ppm (except for the three samples from Subunits 1 and 3B, Figure 5). It is apparent from Figure 5 that there is almost no crystal fractionation within the Upper Igneous Series – otherwise positive correlations between SiO_2 and both Mg and Nd, would be observed. Similarly, the Lower Igneous Series show little indication of crystal fractionation within the series and the less altered samples display narrow ranges in MgO and Nd (5.5-8 wt. % and 20-28 ppm, respectively). In the case of the Tholeiitic Unit, only two altered basalt samples are available. It is therefore difficult to discuss fractionation processes. Heterogeneities within all Series are consistent with different parental melts formed through various degrees of melting of a heterogeneous source (see Shafer et al. 2005).

Distinct protolith compositions were established for each group within the three main Series (Table 1). We chose to calculate the protolith compositions by averaging concentrations of samples with LOI<4% and identified to be relatively little altered on petrographic grounds. Although these samples cannot be considered as completely fresh, by using average data, calculated from multiple samples, we have tried to minimize the primary chemical variations within the different igneous Series. This allows us to define well characterized and appropriate protolith compositions as starting points for our quantifications. The major element concentrations were also recalculated to a H_2O content of 0.5 wt. %, typical in fresh oceanic island basalts (Hauri, 2002). Results of these calculations are presented in Figure 6 (yellow symbols) and Table 4 and these are used in the following sections to calculate gains or losses of elements.

7. Chemical and isotopic characteristics of altered samples and separated minerals

A qualitative estimate of chemical changes can be extracted from plots of selected major and trace element versus La/Yb ratios and by comparing the whole rock compositions of altered and fresh samples (Figure 6, Table 1 and data from Shafer et al., 2005). It is apparent that altered basalts, soil samples and breccia samples from all Series have lower concentrations in SiO_2, CaO (except for one carbonate-bearing breccia sample from Unit 8B), MgO (Figure 5), Sr and Ba. Al_2O_3 concentrations are higher in soil samples but are mostly unchanged in basalt samples as are TiO_2 and Th. The U concentration is higher in some altered basalts from the Upper Igneous Series (Figure 6). Some samples are strongly hydrated (H_2O contents up to ~20%, Table 1) and the impact of dilution cannot be neglected. For example, SiO_2 concentrations can be lowered by up to 10% through addition of water. However, careful examination of the data indicate that dilution alone cannot account for all the variations and most of them are truly related to alteration processes.

Gains and losses of major (g per 100g of protolith) and trace elements (mg per kg of protolith) were calculated using equations from Gresen, (1967) that account for the variations in the chemistry and density of the samples. On average, calculated gains and losses are higher in the High La/Yb group of the Upper Igneous Series (Figure 7a) than in the rest of the basement section (Figure 7b). The largest changes are also calculated for soil and breccia samples (Figures 7a and b). In all Series, the main losses are observed for SiO_2, MgO, CaO and to a lesser extend Na_2O. Fe_2O_3 (Total Fe measured as Fe_2O_3) is mostly gained by samples from the Upper Igneous Series, High La/Yb group (Figure 7a), except the breccia sample from Unit 8B. It is also gained in the High La/Yb group of the Lower Igneous Series but lost by the other groups and in the Tholeiitic Unit. Al_2O_3 is either gained, mainly by soil samples, or lost, mainly by the breccia samples and by basalts samples from the Low La/Yb group of the Lower Igneous Series (Figure 7a and b). Compared to other elements, TiO_2 and more surprisingly K_2O remained almost immobile in all Series. The most significant changes in trace elements are seen for Sr (see also Figure 8) and Ba, which display substantial losses. To a lesser extent Sc and Rb are lost by the altered samples.

Concentrations of Fe^{3+} were measured on all the altered samples and are reported as Fe^{3+}/Fe_T ratios (Figure 8). The highest ratios are seen in the soil and breccia samples as well as in the most altered basalts. Fe^{3+}/Fe_T ratios increase significantly with increasing H_2O content, reaching values of ~1 in the soil samples (Figure 8). In the less altered basalt samples, Fe^{3+}/Fe_T ratios range between ~0.3 and 0.6. No trends are seen downhole indicating oxidizing alteration conditions throughout the entire basement sequence.

The $^{87}Sr/^{86}Sr$ ratios measured on the altered samples were recalculated to an initial value for 56 Ma and are reported together with data on fresh basalts from Shafer et al. (2005, Figures 8 and 9).

Overall, $^{87}Sr/^{86}Sr_{(56\ Ma)}$ ratios vary between ~0.7032 in the least altered samples (Table 1 and data from Shafer et al., 2005) to ~0.706 in the most altered basalts, and soil and breccia samples (Table 1). Clearly, $^{87}Sr/^{86}Sr_{(56\ Ma)}$ ratios are shifted toward more radiogenic values through the alteration process. The Sr concentrations are also strongly influenced by alteration with the most altered basalts, soil and breccia samples having much lower Sr concentrations compared to the freshest samples (Figures 8 and 9). Contrasting behaviour of $^{87}Sr/^{86}Sr$ is observed downhole and an Upper and Lower Alteration Zone are distinguished. Samples from the Upper Alteration Zone display significantly higher $^{87}Sr/^{86}Sr$ ratios (0.7032-0.7062) than samples from the Lower Alteration Zone (0.7032-0.7038). In the Lower Alteration Zone, even the soil samples have $^{87}Sr/^{86}Sr_{(56\ Ma)}$ ratios no higher than 0.7038, whereas soil samples from the Upper Alteration Zone have $^{87}Sr/^{86}Sr_{(56\ Ma)}$ ratios as high as 0.7059 (Table 1, Figures 8 and 9). These two alteration zones cannot, however, be distinguished on the basis of Sr concentrations (Table 1, Figures 8 and 9).

$\delta^{18}O$ measured in both Alteration zones on the most altered basalts, the soil and breccia samples are shifted toward high values (Table 1, Figures 8 and 9). $\delta^{18}O$ in the sequence vary from 8‰, which is significantly above the mantle value expected for fresh igneous rocks (~5.7‰), to 22.5‰ in the soil sample of Subunit 11A (Table 1, Figures 8 and 9). These compositions are typical of clay-rich rocks that have endured fluid rock alteration by low temperature fluids of marine or meteoric origin. At the time of alteration Nintoku island was located close to the tropics (Tarduno et

al., 2003). $\delta^{18}O$ values of meteoric waters above such oceanic tropical islands are only slightly negative because they represent the first condensate of vapour after evaporation from sea water ($\delta^{18}O_{SW}$ = 0‰). It is likely that Nintoku island reached several kilometres in altitude in its early lifetime like the hawaiian volcanoes. Some ^{18}O depletion of meteoric waters is associated with altitude, which may have lowered the $\delta^{18}O$ value of local meteoric waters. Conversely, however, increased relief promotes topographic-driven fluid flow in the volcanic structure, which may result in an enrichment of ^{18}O in waters because of isotopic exchange with rocks at increasing temperature. Consequently, it is difficult to estimate the isotopic composition of the fluids responsible for the alteration or to determine whether alteration took place between basalts and seawater and/or meteoric water solely on the basis of oxygen isotopes. However, as no sample has $\delta^{18}O$ values below 5.7‰, alteration by high temperature exchange with fluids is precluded.

Three carbonate samples were analysed, two of which have $\delta^{13}C$ close to 0‰, $\delta^{18}O$ close to 30‰ and $^{87}Sr/^{86}Sr$ close to 0.7077 (56 Ma seawater) (Table 2, Figures 8 and 9). The remaining sample has a $\delta^{13}C$ of ~ -15‰ (organics, C4 plants), a $\delta^{18}O$ of ~ 25‰ and a $^{87}Sr/^{86}Sr$ ratio of ~0.7035 (Table 2, Figures 8 and 9). The separated clay minerals (kaolinite and/or smectite) have $^{87}Sr/^{86}Sr_{(56\ Ma)}$ ratios varying between ~0.7045 and ~0.7065 (Table 2).

8. Alteration processes and fluids sources

The main features of both Upper and Lower Alteration Zones are summarized in Table 3. Within the Upper Alteration Zone, the elevated Fe^{3+}/Fe_T ratios point to oxidizing conditions for the fluid circulation (Alt, 2003a and references therein). Fe^{3+}/Fe_T ratios in basaltic liquids are usually ~0.1 and are increased by 0.04 to 0.1 during cooling and crystallisation (Christie et al., 1986). The increased Fe^{3+}/Fe_T of the samples cannot, therefore, be explained by these processes. There is a general negative correlation between Sr contents and Sr isotope compositions: the fresh samples have higher Sr contents (between 350 and 650 ppm Sr) with $^{87}Sr/^{86}Sr$ ratios around 0.7035 and the most altered samples have lower Sr contents (<100 ppm) with elevated $^{87}Sr/^{86}Sr$ ratios around 0.706 (Figures 8 and 9, Table 1). The Sr isotope compositions of associated separated clay minerals and carbonate are elevated (0.7045 to 0.7075, Table 2 and Figure 9) indicating their formation from a fluid with a radiogenic Sr isotope signature. The circulating fluid composition that can be deducted from separated minerals is more radiogenic and has a lower Sr concentration than meteoric fluids from present day oceanic islands (river data; Louvat and Allegre, 1997; Louvat and Allegre, 1998). On the other hand, these chemical and isotopic characteristics are consistent with seawater composition at 56 Ma (McArthur et al., 2001) as shown by mixing curves reported in Figure 9. Moreover, separated carbonates have $\delta^{13}C$ composition close to 0‰, consistent with precipitation from seawater. Temperatures of formation for secondary minerals are calculated from mineral-water isotope fractionation factors. Assuming equilibrium with seawater, oxygen isotope data for calcite yield low temperatures between 5 and 15 °C (Clayton et al., 1989; O'Neil et al., 1969). In summary, the Upper Alteration Zone of Hole 1205A basement is similar to, albeit more intensively developed, than alteration of the upper oceanic crust in the cold oxidizing zone (Alt, 2003a)

Whole rock samples from the Lower Alteration Zone, have much less elevated $^{87}Sr/^{86}Sr$ ratios (Table 1, Figures 8 and 9) and their elevated Fe^{3+}/Fe_T rule out fluid circulation under reducing conditions (Figure 8). Separated clay minerals and carbonates show low Sr contents, high $\delta^{18}O$ values, but moderately elevated $^{87}Sr/^{86}Sr$ (Figures 8 and 9, Table 2). $\delta^{13}C$ of a carbonate sample from Subunit 18B is strongly negative at ~-15‰, which is consistent with fractionation by C4 plants and therefore precipitation in a subaerial environment. The most likely explanation to these characteristics is the circulation of a meteoric water-derived fluid with an organic C component. The composition of the subaerial fluid can be a combination of rains eventually mixed with thermal springs (Louvat and Allegre, 1997; Louvat and Allegre, 1998) and sea spray (Whipkey et al., 2000). As there is no evidence of high temperature reactions, and as $\delta^{18}O$ values are elevated, it is likely that thermal spring influence was minor.

Potential fluid compositions are reconstructed using mixing curves between a fresh precursor (Sr ~500 ppm, $^{87}Sr/^{86}Sr$ ~0.7032 and $\delta^{18}O$ ~5.7 ‰) and calculated endmembers representing the

secondary mineral assemblage. These were defined as being mixtures of carbonates and clays minerals with Sr 69 ~ppm, $^{87}Sr/^{86}Sr$ ~0.7068 and $\delta^{18}O$ ~22 ‰ and Sr ~95 ppm, $^{87}Sr/^{86}Sr$ ~0.7045 and $\delta^{18}O$ ~24‰ for the Upper and Lower Alteration Zones respectively. The O isotope compositions of both endmembers are consistent with alteration by either seawater or a meteoric fluid with $\delta^{18}O$ ~0‰. The soil samples from the Upper and Lower Alteration Zones comprise the same minerals as the secondary phases present in the altered basalts (Figure 3) and although alteration is much more intense in these rocks, it mostly occurred under similar conditions.

The Sr isotope signature is partly overprinted in the Upper Alteration Zone by circulation of large amount of seawater whereas the original characteristics are retained in the Lower Alteration Zone. Because Sr contents in the altered rocks are low, Sr is much more susceptible to exchange and be later overprinted through reaction with seawater. Conversely, given that oxygen makes up most of the rock, later seawater alteration is not expected to affect the whole rock isotopic compositions.

9. Gains and losses for Hole 1205A

9.1. Average gain or loss by rock type

We averaged gains and losses calculated for each sample (section 7) to get total gains and losses for each rock type (Figure 10, Table 5). We divided the samples into 6 categories, based on their rock type (soil, breccia, and basalts) and the degree of basalts alteration. The basalts are divided into "slightly altered" (2% < LOI <5%), "moderately altered" (5% < LOI <10%), "highly altered" (10% < LOI <15%) and "intensely altered" (LOI > 15%).

9.2. Lithological proportions in Hole 1205A

We can estimate the gains and losses for each element in the entire basement section with a simple mass balance calculation, which integrates the proportions of each sample type with the gains and losses calculated above. The major problem in doing such calculations is that not all material is recovered when drilling. The basement recovery rate at Hole 1205A is 56.6%, which although relatively high for basement drilling, also implies that almost half of the material was lost. Previous studies that have integrated recovered cores with wireline logs have shown that brittle, weak rock types are preferentially lost during drilling and that simple proportional increase of the recovered proportions to a 100% recovery can result in a significant bias (Barr et al., 2002, and references therein). Soil and breccia are commonly underestimated yet, these are the rock types that show the most dramatic chemical changes during alteration. In the recovered cores, moderately altered basalts are the most abundant lithology together with slightly altered basalts (49.2% and 32.9% respectively, Table 6). 14.6% of highly altered basalts were recovered and low proportions of soil, breccia and intensely altered basalts (1.4%, 1.4% and 0.5% respectively, Table 6). Although these "recovered" proportions are unlikely to be representative of the real basement section, they were included in all calculations because they provide a baseline for comparison with other distributions of rock types. Unfortunately no logging data are available for Hole 1205A and the reconstruction of the basement section must be done without continuous wireline information. We have constructed various hypothetical models of lithological proportions to try to account for the missing material. In Model A, we stated in which proportions the different type of material were recovered taking into account the total length cored in Hole 1205A. In this model, we envisaged that 14% soil, 20% breccia and intensely altered basalts, 50% highly altered basalts, 70% moderately altered basalts and 90% slightly altered basalts were recovered. For example, 8925cm of moderately altered basalts were recovered on a total length of 18128cm. If 70% of this lithology was recovered, then 30% is missing, which represents 3825cm. The resulting thickness of moderately altered basalt will be 12750cm on a total length cored of 28179cm. The proportion of moderately altered basalts of Model A will therefore be 45.3% (Table 6). The other new proportions are: 6.3% soil, 4.5% breccia, 1.6% intensely altered basalt, 18.8% highly altered basalt, and 23.5% slightly altered basalt (Table 6). We also took into account the thicknesses of the different lithologies usually seen on land in comparable climatic settings. Soils profiles have an average

thickness of 1-1.5m (Dia et al., 2005; Kurtz et al., 2001; Monastra et al., 2004; Stewart et al., 2001). Therefore, the recalculated length of soil horizons in our different lithological models was not allowed to exceed this thickness. In Model B, and using the same control parameters, we tried to establish what composed the unrecovered material. Knowing that about 45% material was not recovered, we stated that it was composed of 18% soil, 20% breccia, intensely and highly altered basalt, 12% moderately altered basalt and 10% slightly altered basalt. The recalculated proportions are: 7.4% soil, 8.1% breccia, 7.5% intensely altered basalt, 16.6% highly altered basalt, 35.8% moderately altered basalt and 24.6% slightly altered basalt (Table 6). Finally, we envisaged an extreme model (Model C) in which the lithological proportions are: 10% soil and breccia, 5% intensely altered basalt, 15% highly altered basalt, 35% moderately altered basalt and 25% slightly altered basalt (Table 6).

9.3. Total gains and losses for Hole 1205A

Calculated gains and losses are systematically higher in Models A, B and C than those calculated using the recovered proportions (Table 5, Figure 11). These differences are closely related to the proportions of soil and breccia, which display the highest elemental mobility, with the greatest effects seen for Si, Mg and Sr. However, differences between Models A, B and C are not great. For example, Si losses vary between 6 g/100g in Model A to 7.7 g/100g in Model C (Table 5, Figure 11), which is probably not that significant given the uncertainties in the calculations. In the same manner, the influence on trace element calculated losses is probably also restricted. For example, Sr losses vary between ~198 mg/kg in Model A to ~216 mg/kg in Model C (Table 5, Figure 11).

10. Calculated fluxes for Hole 1205A

Biostratigraphy studies gave an estimated age range of 53.6-54.7 Ma to the sediments overlying the basement (Shipboard Scientific Party, 2002). The seamount basement has been dated by ^{40}Ar-^{39}Ar technique at 55.6±0.2 Ma (Duncan and Keller, 2004). The seamount was therefore exposed to subaerial erosion during 1-2 Ma before it was submerged. It is also clear, from the Sr isotope composition of the Upper Alteration Zone rocks, that the seamount endured seawater alteration. We estimated the duration of this episode to be 1-2 Ma, long enough to allow the overlying sediment pile to build up and act as a barrier to seawater, isolating the volcanic section. Annual fluxes (F) of each element are calculated in g/yr as follow:

$$F = \frac{E \times d \times V}{T}$$

where E represents the calculated gain or loss for a given element (in g/g), d is the average density of the considered lithology (in g/m^3), V is the volcano volume as reported in the literature (in m^3) and T is the time during which the edifice was subject to alteration (in yr). We first used a global ocean island emplacement rate of 0.01 km^3/yr (Bargar and Jackson, 1974), which corresponds to a volume of 50×10^3 km^3. However, more recent studies indicate that this emplacement rate may be higher, up to 0.06 km^3/yr (Robinson and Eakins, 2005; Van Ark and Lin, 2004; Vidal and Bonneville, 2004) corresponding to a volume of 180×10^3 km^3. In both calculations, we used duration of 3 Ma for the alteration episode. We also made the assumption that the whole seamount was altered to a similar degree as the rocks analysed from Hole 1205A. Although this makes our calculated annual fluxes maxima, as the great majority of the seamount was never sub-aerially exposed, we consider this assumption a reasonable starting point. Future work will better estimate what proportions of emergent seamounts undergo submarine and sub-aerial weathering and if some higher temperature fluid alteration occurred within the interior of the seamount. Calculated annual fluxes depend on the emplacement rate and, to a lesser extent, on the chosen lithological proportion model (Figure 12). There are net losses of SiO_2 (0.2-1.2$\times10^{13}$ g/yr), MgO (0.6-4.3$\times10^{12}$

g/yr), CaO (0.9-6×10^{12} g/yr) and Na_2O (0.2-1.3×10^{12} g/yr). Conversely, there is a net uptake of Fe_2O_3, between 2.5×10^{11} g/yr and 2.8×10^{12} g/yr (Figure 12). For the trace elements, the major fluxes are seen for Sr (net loss 0.7-3.7×10^9 g/yr) and Ba (net loss 0.2-1.2×10^9 g/yr). To a lesser extend, losses are seen for Rb (0.5-4.5×10^7 g/yr), Y (0.1-4.8×10^7 g/yr). A small gain in U is also observed (0.2-1.9×10^6 g/yr) (Figure 12). Because there is such sparse data on the alteration and weathering of ocean islands, it is very difficult to calculate rigorous statistical limits for the chemical fluxes. However, using different basement models (i.e. different proportions of rock types) and different emplacement rates give a range of estimates for each element. It is also likely that these two parameters will have much greater influence on chemical fluxes than variations of chemical mobility within the different rock types.

11. Comparison with mid-ocean ridge flank fluxes

Here we make some comparison between fluxes calculated for Nintoku seamount and those reported for mid-ocean ridge off-axis low temperature fluid circulation settings (Table 7). The generally reported features are the uptake of Si, Al, Mg, K, Na, Rb, Cs, and U by oceanic crust (Alt, 2003a, b; Schramm et al., 2005; Staudigel et al., 1996 ; see also Table 7). It has also been shown recently that oceanic crust may be a sink for Ba (Schramm et al., 2005) and a source of Sr (Wheat and Mottl, 2000). Staudigel et al. (1996) used a composite approach to calculate fluxes in DSDP Sites 417 and 418, with significant fluxes for SiO_2 (42.6×10^{12} g/yr), Al_2O_3 (69.9×10^{12} g/yr), CaO (77.3×10^{12} g/yr) and K_2O (19.5×10^{12} g/yr). Using a different approach, Spivack and Staudigel (1994) calculated a K flux of ~16×10^{12} g/yr at the same sites. Chemical fluxes were also calculated for Hole 504B using different methods such as a mass balance approach (similar to our method; Alt et al., 1986) or a composite approach (Bach et al., 2003) and on other sites in ridge flank settings (Juan de Fuca Ridge or the eastern flank of the East Pacific Rise, Bach et al., 2003; Schramm et al., 2005; Wheat and Mottl, 2000; Table 7). The chemical behaviour of most elements are consistent from one site to another but the magnitude of fluxes can be highly variable (Table 7). These differences may be related to the age of the oceanic crust at the different sites (6.9 Ma for Hole 504B; Alt et al., 1986 and 118 Ma for Sites 417/418, Staudigel et al., 1996, for example), as well as contrasting volcanologic, sedimentologic and hydrogeologic settings but the influence of these parameters is poorly understood. Similar chemical behaviour is observed for Hole 801C in old (170 Ma) oceanic crust (Alt and Teagle, 2003; Kelley et al., 2003), but chemical fluxes have not yet been calculated.

The comparison of both setting indicate that Ca has the same behaviour, being depleted in altered rocks (resulting in a flux to the oceans). It should be recognized, however, that our calculated flux for Ca is a maximum value. We are interested here in establishing preliminary estimates and hydrothermal veins are not accounted for in our study. It is possible that some Ca is reprecipitated as veins but Sr isotope compositions suggest that most of the Ca was derived from seawater. Conversely to “normal” oceanic crust, Nintoku seamount acted as a source of Si, Mg, Na, and Ba. Al, K, Cs, Rb and U remained almost immobile and the seamount was a sink for Fe. A likely explanation for this difference is that Nintoku seamount was first altered in a subaerial setting and its major geochemical characteristics are inherited from that episode. Subsequent seawater alteration is not extensive enough to completely overprint the subaerial alteration. Soil samples are significantly depleted in Si and Mg compared to the basalts (Figures 5 and 6). Circulation of subaerial fluid likely promoted the destabilisation of glass and the most easily altered minerals to form soil horizons. These were later leached during weathering and large amounts of Si were provided to the hydrological system. However, the soil from Unit 7 (Upper Alteration Zone) is less depleted in Si than the other soil samples (Figures 5 and 6, Table 1). This may reflect the influence of the later seawater circulation process that entrains the uptake of Si like in other oceanic settings at low temperature (Alt, 2003a; Alt, 2003b; Schramm et al., 2005; Staudigel et al., 1996). However, Si leaching during subaerial weathering is more extensive and dominates over the uptake of Si during submarine alteration. The result is a net loss of Si by the seamount. Soil samples are

enriched in Al that can be related to the occurrence of kaolinite (Figure 3, Table 1). The altered basalts and the breccia samples are variably depleted in Al, likely related to plagioclase alteration. It is possible that some Al was transferred from the basalts to the soils via the circulating fluid. As a result, Al was neither gained nor lost in the overall chemical flux. We also observe a dual behaviour of K in the altered samples. Samples from the Upper Alteration Zone have higher concentrations in K whereas samples from the lowermost part of the hole are depleted. K was probably leached during the subaerial weathering episode, as were all highly mobile elements but was incorporated in newly formed secondary minerals during seawater circulation. As K is more mobile than Si it was likely more extensively mobilised during the submarine episode, but this results in neither a positive nor a negative chemical flux for K. The seamount acts as a sink for Fe. All soil and altered samples are enriched in Fe compared to the least altered samples. Unless the circulating fluid (meteoric water) delivered large amounts of Fe, it is probable that Fe was passively accumulated.

The largest trace element fluxes are observed for Ba and Sr. It appears that seamount alteration may represent an important source for these two elements in seawater. Previous studies have demonstrated that it is difficult to balance the modern ^{87}Sr oceanic budget because the radiogenic inputs from rivers are much larger than more primitive Sr inputs from the hydrothermal alteration of the oceanic crust (Davis et al., 2003). The Sr isotopic exchanges observed in altered basalts, soils and breccias, from Nintoku seamount, indicate that the alteration of oceanic islands can release significant amounts of Sr with a basalt-like Sr isotope ratios to the oceans, and that this input can partially address the apparent inbalance in the oceanic Sr budget.

12. Conclusion

The Nintoku seamount grew to sub-aerial emergence where it was weathered and eroded and was subsequently submerged and subjected to seawater circulation. The cored seamount section comprises two Igneous Series of alkali basalts separated by a tholeiitic unit. These units are composed of variably altered basalts and associated breccia and soils horizons. To establish preliminary estimates of the potential influence of ocean island erosion and alteration on the global oceanic chemical budget we have attempted to quantify chemical fluxes between seamounts and the oceans. The secondary mineral assemblage of Hole 1205A shows no trends downhole and comprises mainly Fe-oxyhydroxides, clay minerals, Ca-carbonates and minor zeolites. Soils are composed of variably altered basaltic clasts in a matrix of clay minerals and Fe-oxides. We distinguish an Upper Alteration Zone in which $^{87}Sr/^{86}Sr$ ratios are close to 56 Ma seawater from a Lower Alteration Zone in which $^{87}Sr/^{86}Sr$ ratios are less elevated. In both zones, Fe^{3+}/Fe_T and $\delta^{18}O$ are strongly elevated compared to primary igneous values. The Lower Alteration Zone likely reflects interaction with a subaerial oxidizing fluid at low temperature and probably retains ed most of the signature of the initial phase of subaerial weathering. The Upper Alteration Zone was altered through circulation of large quantities of cold, oxidizing seawater that partly overprints the subaerial weathering chemical characteristics.

We used the primary geochemical characteristics of the freshest basalts recovered to define protolith compositions and to calculate gains and losses of major and trace elements. Compared to fresher samples, altered basalt, soil and breccia are mainly depleted in Si, Mg, Ca, Na, Sr, Rb and Ba and enriched in Fe. As the recovery at Hole 1205A is not complete, we have constructed a variety of lithological proportion models to account for the missing material and calculated global gains and losses for the basement section. We also calculated annual chemical fluxes for Hole 1205A using different magma emplacement rates for ocean islands. Our calculations indicate that the seamount released Si, Ca, Mg, Sr and Ba and retained for Fe, in contrast to the chemical changes observed during low temperature alteration in mid-ocean ridge settings. We interpret this difference as the result of the subaerial weathering episode, which was later only partially modified through circulation of seawater. Most importantly, our results indicate that erosion and alteration of an oceanic island can have a significant impact on the chemical budget of oceans. Although further work is needed to better constrain these fluxes, it is clear from our study that alteration and

weathering of ocean islands is a factor that should not be neglected when considering global chemical budget of oceans.

Acknowledgments:

We thank the ODP Leg 197 shipboard party, the laboratory technicians and crew of the *JOIDES Resolution.* Thanks to Matthew Cooper, Andrew Milton, Timothy Brewer, Marcel Bohn, Jo Cotten and Jean Cornichet, at respectively the Southampton Oceanography Centre, the University of Leicester, Ifremer, the University of Brest and the University of Rennes1 for help during the analytical processes. We are grateful to J. Alt and C. Laverne for constructive reviews. SR was supported at the Southampton Oceanography Centre by a Marie Curie Fellowship (HPMF-CT-2000-00958). This work was supported through ODP France (INSU group ad hoc "OCEANS") and ODP UK (NERC grant NER/T/S/2001/01237). This research uses samples and data provided by the ODP, which is sponsored by the US National Science Foundation, and participating countries under the management of Joint Oceanographic Institutions.

References:

Alt, J.C., 1995. Subseafloor processes in mid-ocean ridge hydrothermal system. In: S. Humphris et al. (Editors), *Seafloor hydrothermal systems: physical, chemical, biological and geological interactions*. AGU Monograph, pp. 85-114.

Alt, J.C., 2003a. Alteration of the upper oceanic crust: mineralogy, chemistry and processes. In: H. Elderfield and E. Davis (Editors), *Hydrogeology of the Oceanic Lithosphere.* Cambridge Press, Cambridge.

Alt, J.C., 2003b. Hydrothermal fluxes at mid-ocean ridges and on ridge flanks. *C.R.A.S. Geosciences*, 335: 853-864.

Alt, J.C. et al., 1996. Ridge flank alteration of upper ocean crust in the eastern pacific: synthesis of results for volcanic rocks of holes 504B and 896A. In: J.C. Alt, H. Kinoshita, L.B. Stokking and P.J. Mickael (Editors), Alt, J.C. Kinoshita, H. Stokking, L.B. Mickael, P.J. Ocean Drilling Program, College Station, TX, pp. 435-450.

Alt, J.C., Honnorez, J., Laverne, C. and Emmermann, R., 1986. Hydrothermal alteration of a 1 km section through the upper oceanic crust. DSDP Hole 504B: Mineralogy, chemistry and evolution of seawater-basalt interactions. *J. Geophy. Res.*, 91: 309-335.

Alt, J.C. and Teagle, D.A.H., 1999. The uptake of carbon during alteration of ocean crust. *Geochim. Cosmochim. Acta*, 63(10): 1527-1535.

Alt, J.C. and Teagle, D.A.H., 2003. Hydrothermal alteration of upper oceanic crust formed at a fast-spreading ridge: mineral, chemical and isotopic evidence from ODP Site 801. *Chem Geol*, 201: 191-211.

Bach, W., Peucker-Ehrenbrink, B., Hart, S.R. and Blusztajn, J.S., 2003. Geochemistry of hydrothermally altered oceanic crust: DSDP/ODP Hole 504B - Implications for seawater-crust exchange and Sr- and Pb-isotopic evolution of the mantle. *Geochem. Geophys. Geosyst.*, 4(3): 2002GC000419.

Bargar, K. and Jackson, E., 1974. Calculated volumes of individual shield volcanoes along the Hawaiian-Emperor chain. *J. Res. U.S. Geol. Surv.*, 2: 545-550.

Barr, S.R., Révillon, S., Brewer, T.S., Harvey, P.K. and Tarney, J., 2002. Determining the inputs to the Mariana Subduction Factory: using core-log integration to reconstruct basement lithology at ODP Hole 801C. Geochem. Geophys. Geosyst., 3(11): 2001GC000255

Brewer, T.S. et al., 1998. Ocean floor volcanism: constraints from the integration of core and downhole logging measurments. In: P.K. Harvey and M.A. Lovell (Editors), *Core-Log integration.* Geol. Soc. London Spec. Publ., London, pp. 341-362.

Christie, D.M., Carmichael, I.S.E. and Langmuir, C.H., 1986. Oxidation states of mid-ocean ridge basalt glasses. *Earth Planet. Sci. Lett.*, 79: 397-411.

Clayton, R.N., Goldschmidt, J.R. and Mayada, T.K., 1989. Oxygene isotopes fractionation in quartz, albite, anorthite and calcite. *Geochim. Cosmochim. Acta*, 53: &25-734.

Clayton, R.N. and Mayeda, T.K., 1963. The use of bromine pentafluorine in the extraction of oxygen from oxydes and silicates for isotopic analysis. *Geochim. Cosmochim. Acta*, 27: 43-52.

Cotten, J. et al., 1995. Origin of anomalous rare-earth element and yttrium enrichments in subaerially exposed basalts: evidence from French Polynesia. *Chem Geol*, 119: 115-138.

Dalrymple, G.B., Lanphere, M.A. and Clague, D.A., 1981. Conventional and ^{40}Ar-^{39}Ar ages of volcanic rocks from Ojin (site 430), Nintoku (site 432), Suiko (site 433) seamounts and the chronology of volcanic propagation along the Hawaiian-Emperor chain. In: E.D. Jackson and I. Koizumi (Editors), *Initial report of the Deep Sea Drilling Project*. US Government Printing Office, Washington, pp. 659-676.

Davis, A.C., Bickle, M.J. and Teagle, D.A.H., 2003. Imbalance in the oceanic strontium budget. *Earth Planet. Sci. Lett.*, 211: 173-187.

Dia, A., Chauvel, C., Bulourde, M. and Gérard, M., 2005. Eolian contribution to soils on Mount Cameroon: Isotopic and trace element records. *Chem Geol*, in press.

Duncan, R.A. and Keller, R.A., 2004. Radiometric ages for basement rocks from the Emperor Seamounts, ODP Leg 197. *Geochem. Geophys. Geosyst.*, 5(8): 2004GC000704.

Elderfield, H. and Schultz, A., 1996. Mid-ocean ridge hydrothermal fluxes and the chemical composition of the oceans. *Annu. Rev. Earth Planet. Sc*, 24: 191-224.

Gresen, R.L., 1967. Composition-volume relationships of metasomatism. Chem. Geol., 2: 47-55.

Hauri, E., 2002. SIMS analysis of volatiles in silicate glasses, 2: isotopes and abundances in Hawaiian melt inclusions. *Chem Geol*, 183(1-4): 115-141.

Jackson, E.D., Koizumi, I. and et al., 1980. Init. Repts. DSDP, 55. U.S. Govt. Printing Office, Washington.

Kelley, K.A., Planck, T., Ludden, J. and Staudigel, H., 2003. Composition of Altered Oceanic Crust at ODP Sites 801 and 1149. Geochem. Geophys. Geosyst., 4(6): 2002GC000435

Kurtz, A.C., Derry, L.A. and Chadwick, O.A., 2001. Accretion of Asian dust to Hawaiian soils: Isotopic, elemental, and mineral mass balances. *Geochim Cosmochim Acta*, 65(12): 1971-1983.

Laverne, C., Agrinier, P., Hermitte, D. and Bohn, M., 2001. Chemical fluxes during hydrothermal alteration of a 1200-m long section of dikes in the oceanic crust, DSDP/ODP Hole 504B. *Chem. Geol.*, 181: 73-98.

Louvat, P. and Allegre, C.J., 1997. Present denudation rates on the island of Reunion determined by river geochemistry: basalt weathering and mass budget between chemical and mechanical erosion. *Geochim. Cosmochim. Acta*, 61(17): 3645-3669.

Louvat, P. and Allegre, C.J., 1998. Riverine erosion rates on Sao Miguel volcanic isalnd, Azores archipelago. *Chem. Geol.*, 148: 177-200.

Ludden, J.N. and Thompson, G., 1978. Behaviour of rare earth elements during submarine weathering of tholeiitic basalt. *Nature*, 274: 147-149.

McArthur, J.M., Howarth, R.J. and Bailey, T.R., 2001. Strontium Isotope Stratigraphy: LOWESS Version3: Best fit to the marine Sr-isotope curve for 0-509 Ma and accompanying look up table for deriving numerical age. *The Journal of Geology*, 109: 155-170.

Monastra, V., Derry, L.A. and Chadwick, O.A., 2004. Multiple sources of lead in soils from a Hawaiian chronosequence. *Chem Geol*, 209: 215-231.

Mottl, M.J. and Wheat, C.G., 1994. Hydrothermal circulation through mid-ocean ridge flanks: Fluxes of heat and magnesium. *Geochim. Cosmochim. Acta*, 58: 2225-2237.

O'Neil, J.R., Clayton, R.N. and Mayeda, T.K., 1969. Oxygen isotopes fractionation in divalent metal carbonates. *J Chem. Phys.*, 51: 5547-5558.

Palmer, M.R. and Edmond, J.M., 1989. The Strontium isotope budget of the modern ocean. *Earth Planet. Sci. Lett.*, 92: 11-26.

Robinson, J.E. and Eakins, B.W., 2005. Calculated volumes of individual shield volcanoes at the young end of the Hawaiian Ridge. J. *Volc. Geotherm. Res.*, in press.

Schramm, B., Devey, C.W., Gillis, K.M. and Lackschewitz, K., 2005. Quantitative assessment of chemical and mineralogical changes due to progressive low-temperature alteration of East Pacific Rise basalts from 0 to 9 Ma. *Chem Geol*, 218: 281-313.

Shafer, J.T., Neal, C.R. and Regelous, M., 2005. Petrogenesis of Hawaiian postshield lavas: Evidence from Nintoku Seamount, Emperor Seamount chain. *Geochem. Geophys. Geosyst.*, 6: 2004GC000875.

Shipboard Scientific Party, 2002. Site 1205. In: J.A. Tarduno, Duncan, R.A., Scholl, D.W., et al., (Editor), *Proc.ODP, Init. Repts., 197*, [CD-ROM]. Available from: Ocean Drilling Program,. Texas A&M University, College Station TX 77845-9547, USA.

Spivack, A.J. and Staudigel, H., 1994. Low temperature alteration of the upper oceanic crust and the alkalinity budget of seawater. *Chem Geol*, 115: 239-247.

Staudigel, H., Plank, T., White, W. and Schmincke, H.U., 1996. Geochemical fluxes during seafloor alteration and the basaltic upper oceanic crust: DSDP Sites 417 and 418. In: G.E. Bebout, D.W. Scholl, S.H. Kirby and J.P. Platt (Editors), *Subduction top to bottom.* AGU Monograph.

Stewart, B.W., Capo, R.C. and Chadwick, O.A., 2001. Effects of rainfall on weathering rate, base cation provenance, and Sr isotope composition of Hawaiian soils. *Geochim. Cosmochim. Acta*, 65(7): 1087-1099.

Tarduno, J.A., et al., 2003. The Emperor Seamounts: Southward Motion of the Hawaiian Hotspot Plume in Earth's Mantle. *Science* 301: 1064-1069.

Teagle, D.A.H., Bickle, M.J. and Alt, J.C., 2003. Recharge Flux to ocean-ridge black smoker systems: a geochemical estimate from ODP Hole 504B. *Earth Planet. Sci. Lett.*, 210: 81-89.

Van Ark, E. and Lin, J., 2004. Time variations in igneous volume flux of the Hawaii-Emperor hot spot seamount chain. *J Geophys Res*, 109(B11401).

Vidal, V. and Bonneville, A., 2004. Variations of the Hawaiian hot spot activity revealed by variations in the magma production rate. *J Geophys Res*, 109(B03104).

Wheat, C.G. and Mottl, M.J., 2000. Composition of pore and spring waters from Baby Bare: Global implications of geochemical fluxes from a ridge flank hydrothermal system. *Geochim. Cosmochim. Acta*, 64(4): 629-642.

Whipkey, C.E., Capo, R.C., Chadwick, O.A. and Stewart, B.W., 2000. The importance of sea spray to the cation budget of a coastal Hawaiian soil: a strontium isotope approach. *Chem. Geol.*, 168: 37-48.

Figure and Table captions:

Figure 1: ODP Leg 197 sites in the Emperor Seamounts with ages of selected sites (Ma) and seafloor magnetic isochrons.

Figure 2: Basement lithostratigraphy of Hole 1205A. From left to right are reported Core names Recovery (black intervals represent the recovered proportions), Lithology, Unit, Rock name, Igneous series, Alteration zone, Alteration degree, alteration assemblage, and Vesicle filling. Green: sediment, Red: soil, Yellow: breccia and Blue: basalt. Sp: sparsely, Mod: moderately, Hi: highly. Plag: plagioclase, Ol: olivine. TU: Tholeiitic Unit. Alteration degree is graded on a scale from 0 to 5 based on alteration product volume as follow: 0 = unaltered (<2%), 1 = slightly altered (2%-5%), 2 = moderately altered (5%-10%), 3 = highly altered (10%-15%), 4 = very highly altered (15%-20%), 5 = intensely altered (>20%).

Figure 3: X-Ray Diffractograms of soil samples from Hole 1205A.

Figure 4: La/Yb versus depth of fresh (data from Shafer et al., 2005) and altered samples from ODP Hole 1205A. Following Shafer et al. (2005) the basement section is divided into three main Series (Upper and Lower Igneous Series and Tholeiitic Unit). Based on La/Yb ratios variations we

also distinguished two groups (High La/Yb and Low La/Yb) in each of the Upper and Lower Igneous Series.

Figure 5: SiO_2 (wt. %) versus MgO (wt. %) and Nd (ppm) of fresh and altered samples from ODP Hole 1205A. Symbols are identical to Figure 4.

Figure 6: La/Yb versus SiO_2 (wt. %), CaO (wt. %), TiO_2 (wt. %), Al_2O_3 (wt. %), Th (ppm), U (ppm), Sr (ppm) and Ba (ppm) of fresh and altered samples from ODP Hole 1205A. Also shown are the calculated protolith compositions for each group of samples (yellow symbols).

Figure 7: Gains or losses of element (major element in g/100 g, trace element in mg/kg of the parent rock) calculated after the method of Gresen (1967). Due to the number of samples, we separated the High La/Yb group of the Upper Igneous Series (Figure 7a) from the other groups (Figure 7b). Blue symbols represent basalt samples in both figures.

Figure 8: ΔSr, $^{87}Sr/^{86}Sr_{(56\ Ma)}$, $\delta^{18}O$ (‰) and Fe^{3+}/Fe_T versus depth (mbsf) of some fresh and altered samples from Hole 1205A. Sr and O isotopes compositions of separated clay and carbonate minerals are also plotted. ΔSr (ppm) is calculated as $[Sr]_{altered\ sample} - [Sr]_{protolith}$.

Figure 9: (a) Sr (ppm) versus $^{87}Sr/^{86}Sr_{(56\ Ma)}$ ratios of samples from both Upper and Lower Alteration Zones and separated carbonate and clay minerals from Hole 1205A. Also plotted are mixing lines, illustrating the different alteration processes, between a fresh precursor (Sr 500 ppm and $^{87}Sr/^{86}Sr$ 0.7032) and fluids: seawater at 56 Ma (Sr 8 ppm and $^{87}Sr/^{86}Sr$ 0.7077) and a subaerial (meteoric) fluid (Sr 95 ppm $^{87}Sr/^{86}Sr$ 0.70447). Ticks represent 10% mixing increments. (b) $\delta^{18}O$ (‰) versus $^{87}Sr/^{86}Sr_{(56\ Ma)}$ ratios of samples from both Upper and Lower Alteration Zones and separated carbonate and clay minerals from Hole 1205A. The Upper Alteration Zone reflects interaction with a seawater-dominated fluid and the Lower Alteration Zone reflects interaction with a subaerial-dominated fluid. Mixing line were calculated between a fresh precursor ($\delta^{18}O$ 5.7 ‰, Sr 500 ppm and $^{87}Sr/^{86}Sr$ 0.7032) and chosen endmembers representing mixtures of carbonates and clays minerals with Sr 69 ppm, $^{87}Sr/^{86}Sr$ 0.7068 and $\delta^{18}O$ 22 ‰ and Sr 95 ppm, $^{87}Sr/^{86}Sr$ 0.70447 and $\delta^{18}O$ 24‰ for the Upper and Lower Alteration Zones respectively. Ticks represent 10% mixing increments.

Figure 10: Average gains and losses of major (g/100g) and trace (mg/kg) elements for each lithology recovered in Hole 1205A basement. Basalt samples are grouped following their LOI value (as a measure of their degree of alteration).

Figure 11: Global gains and losses of major (g/100g) and trace (mg/kg) elements for Hole 1205A. Four lithological proportions models were used for the calculations. The first one used the proportions of soil, breccia and basalts as recovered in the cores. See Table 6 for lithological assemblage in each model and text for details.

Figure 12: Calculated fluxes of elements in g/yr for Nintoku seamount (Hole 1205A) using emplacement rates of 0.01 km^3/yr and 0.06 km^3/yr and our four proposed lithological proportions models. See text for details.

Table 1: Major and trace element concentrations in samples from ODP Hole 1205A. Alteration degree is graded on a scale from 0 to 5 based on alteration product volume as follow: 0 = unaltered (<2%), 1 = slightly altered (2%-5%), 2 = moderately altered (5%-10%), 3 = highly altered (10%-15%), 4 = very highly altered (15%-20%), 5 = intensely altered (>20%). Major elements and trace

element in italics were measured by ICP-AES. The remaining was measured by ICP-MS. See also "Analytical techniques". Initial $^{87}Sr/^{86}Sr$ ratios were calculated using an age of 56 Ma.

Table 2: Sr, C and O isotope compositions of carbonates and clay minerals separates from Nintoku Seamount (ODP Site 1205). Sr concentrations were measured by ICP-MS at SOC.

Table 3: Main igneous and alteration characteristics of ODP Hole 1205A samples. n.a.: not applicable; n.d.: not determined. Data in italic are from Shafer et al. (2005).

Table 4: Calculated protolith compositions and errors used in the calculations

Table 5: Average gains and losses for each lithology recovered at Hole 1205A and global gains and losses calculated for the all basement sequence using different lithological proportions models. n: number of samples. Negative numbers indicate losses by the latered samples whereas positive numbers indicate gains by the altered samples.

Table 6: Lithological proportions used in the gain/loss and the flux calculations.

Table 7: Comparison of geochemical fluxes related to low temperature alteration in ridge settings (Hole 504B, Sites 417/418, Juan de Fuca Ridge and EXCO zone eastern flank of the east pacific rise) and on Nintoku seamount (Min: minimum ; Max: maximum values calculated in this study). Note that positive values indicate flux into the oceans, while negative values indicate flux into crust. LT : low temperature. Other data from (a) Bach et al. (2003); (b) Alt (2003b); (c) Staudigel et al. (1996); (d) Spivack and Staudigel (1994); (e) Wheat and Mottl (2000); (f) Schramm et al. (2005).

ODP Leg 197, Hole 1205A																			
	19R-4	**19R-4**	**20R-6**	**21R-2**	**21R-2**	**23R-1**	**23R-4**	**24R-3**	**25R-2**	**26R-1**	**26R-2**	**33R-4**	**34R-1**	**34R-4**	**34R-4**	**35R-1**	**35R-4**	**35R-5**	**36R-1**	**36R-6**
Interval (cm)	10-22	66-71	97-99	42-46	107-112	16-20	90-92	44-47	70-73	13-18	124-133	36-38	106-110	94-100	126-130	56-58	91-110	24-31	33-39	9-11
Depth	114.2	114.7	127.5	131.1	131.7	139.1	143.8	151.9	159.9	167.8	170.4	229.3	236.1	239.9	240.2	245.2	248.9	249.5	254.6	260.7
Unit	7	8A	8A	8B	9	10	10	10	11A	11B	11B	18A	18B	18B	18B	19A	19B	19C	20	20
Rock type	Soil	Plag-Ol bas	Plag-Ol bas	Breccia	Aphy basalt	Plag-Ol bas	Plag-Ol bas	Plag-Ol bas	Soil	Aphy basalt	Aphy basalt	Soil	Aphy basalt	Aphy basalt	Aphy basalt	Soil	Ol basalt	Breccia	Ol basalt	Ol basalt
Igneous Series	Upper	Upper	Upper	Upper	Upper	Upper	Upper	Upper	Upper	Upper	Upper	Upper	Upper	Upper	Upper	Tholeiitic	Tholeiitic	Tholeiitic	Lower	Lower
Alteration	5	4	1	5	2	4	4	3	5	3	3	5	4	3	4	5	3	5	3	1
Density		2.14	2.97	2.39	2.95	2.47	2.33	2.63		2.57	2.64		2.31	2.54	2.02		2.77	1.95	2.5	2.9
SiO_2	36.00	34.50	45.75	27.70	45.15	41.20	35.30	42.50	33.00	41.20	41.00	30.60	41.25	41.20	36.10	28.70	44.00	33.15	39.50	45.35
TiO_2	2.72	2.60	2.55	2.07	2.39	2.91	3.35	3.10	2.39	2.68	2.62	3.82	1.90	2.09	2.02	1.74	1.25	3.82	2.85	2.49
Al_2O_3	17.00	15.25	14.50	10.90	15.20	16.92	16.45	15.75	17.90	15.82	15.30	19.70	13.15	14.48	14.98	19.30	13.70	21.30	14.80	13.75
FeO	1.18	0.81	8.55	0.27	4.50	1.98	1.18	1.88	0.81	4.51	5.40	0.81	5.06	2.25	0.99	0.18	6.02	0.27	2.80	9.02
Fe_2O_3	14.84	15.45	5.85	11.85	8.79	14.50	18.49	14.91	16.45	9.69	9.55	17.75	7.18	13.20	14.70	16.60	6.26	22.80	12.83	4.78
MnO	0.11	0.14	0.19	0.19	0.17	0.17	0.21	0.16	0.10	0.23	0.29	0.20	0.20	0.15	0.19	0.07	0.13	0.25	0.19	0.18
MgO	1.71	1.92	6.05	2.76	6.05	2.06	1.98	3.77	1.88	5.50	6.00	1.13	8.97	6.20	4.47	0.96	10.08	1.75	5.39	8.09
CaO	2.40	4.85	8.50	16.40	8.55	3.21	0.78	4.95	0.55	4.80	5.40	1.24	5.70	6.00	3.40	1.50	7.85	1.99	6.15	8.42
Na_2O	1.88	1.68	3.10	1.24	3.03	4.67	1.63	3.36	1.29	2.44	2.24	1.01	2.05	2.30	2.18	0.99	2.02	1.12	1.82	2.89
K_2O	1.49	1.53	0.75	1.04	0.74	1.53	1.30	1.30	0.70	0.84	0.75	0.19	0.48	0.68	0.46	0.29	0.13	0.22	0.76	0.69
P_2O_5	0.45	0.42	0.37	0.53	0.32	0.40	0.31	0.34	0.09	0.36	0.38	0.11	0.27	0.32	0.58	0.12	0.12	0.12	0.57	0.37
H_2O	19.09	18.44	2.55	18.94	3.76	11.38	18.51	7.31	24.23	10.93	9.87	22.76	12.61	10.47	19.35	28.77	6.95	12.38	11.12	2.37
CO_2	1.22	2.97	0.19	10.91	0.16	0.07	0.13	0.13	0.13	0.11	0.11	0.28	0.35	0.32	0.23	0.16	0.20	0.12	0.38	0.17
Total	100.09	100.57	98.90	104.81	98.82	101.00	99.61	99.46	99.52	99.12	98.91	99.60	99.17	99.67	99.65	99.38	98.71	99.29	99.16	98.56
Fe^{3+}/Fe_T	0.92	0.94	0.38	0.98	0.64	0.87	0.93	0.88	0.95	0.66	0.61	0.95	0.56	0.84	0.93	0.99	0.48	0.99	0.80	0.32
La/Yb	10.89	9.05	9.12	8.30	9.42	8.19	9.10	8.74	8.41	9.35	9.58	9.84	9.02	9.07	8.88	3.04	4.75	22.69	13.67	12.55
S	7	18	35	19	16	4	33	39	88	25	18	28	7	9	10	26	2	4	5	11
V	*273*	*235*	*290*	*172*	*320*	*310*	*370*	*395*	*220*	*380*	*350*	*265*	*225*	*240*	*226*	*310*	*229*	*295*	*470*	*293*
Cr	*68*	*64*	*49*	*30*	*118*	*97*	*63*	*46*	*215*	*153*	*156*	*365*	*248*	*268*	*264*	*460*	*468*	*400*	*300*	*259*
Co	*44*	*30*	*42*	*34*	*50*	*39*	*40*	*53*	*53*	*53*	*51*	*74*	*48*	*75*	*57*	*51*	*62*	*75*	*65*	*56*
Ni	*65*	*50*	*41*	*51*	*74*	*52*	*53*	*54*	*108*	*98*	*92*	*210*	*165*	*195*	*205*	*255*	*325*	*360*	*315*	*209*
Sc	16.21	20.34	18.26	14.95	19.62	17.11	21.21	22.03	20.52	17.14	20.22	18.40	14.54	14.64	16.58	19.75	13.93	17.93	17.86	19.64
Rb	17.61	22.20	9.92	13.12	8.84	9.22	15.45	17.39	6.83	8.05	8.30	1.82	5.51	9.28	4.06	8.15	0.42	4.46	9.15	8.86
Sr	67.82	57.61	249.74	70.72	296.89	169.96	93.93	299.53	41.59	140.20	151.49	72.31	147.09	205.38	149.45	61.20	179.94	133.58	149.74	445.14
Y	22.69	28.38	22.86	28.87	21.02	19.60	21.96	24.11	18.15	18.25	21.44	20.89	17.27	21.07	20.53	17.97	14.08	23.56	24.42	20.67
Zr	128.47	142.10	125.09	119.68	117.22	136.26	132.74	132.62	103.36	101.08	111.17	198.65	97.25	114.80	102.63	51.02	52.51	163.45	141.34	135.93
Nb	19.83	20.24	17.97	16.85	17.19	22.33	21.61	20.82	16.29	15.71	18.23	25.02	15.17	16.48	15.24	4.97	5.83	24.70	21.25	22.35
Cs	0.27	0.26	0.11	0.10	0.09	0.37	0.39	0.24	0.12	0.13	0.06	0.13	0.02	0.12	0.03	0.25	0.00	0.23	0.06	0.05
Ba	110.78	98.73	164.02	79.20	165.60	142.17	121.56	187.89	89.09	161.01	146.80	28.69	110.57	133.46	89.52	12.53	46.27	64.07	150.82	210.22
La	17.34	18.90	15.44	16.55	14.53	13.15	15.69	15.37	13.16	15.51	16.54	18.35	12.56	14.23	14.48	7.18	5.12	42.23	21.51	18.74
Ce	40.26	42.72	36.15	36.36	34.25	30.70	34.91	36.46	30.79	36.12	37.01	41.36	29.02	32.76	32.70	22.23	12.06	58.67	46.11	42.50
Pr	4.19	4.89	3.81	4.35	3.72	3.43	3.96	3.98	3.31	3.97	4.05	3.80	3.24	3.56	3.54	2.78	1.45	7.37	5.02	4.49
Nd	19.67	22.66	18.21	20.02	17.41	16.34	18.87	19.05	15.53	18.31	18.97	17.79	14.76	16.79	16.85	13.84	7.25	31.64	21.77	19.97
Sm	4.61	5.49	4.27	4.87	4.14	4.01	4.51	4.56	3.77	4.51	4.48	4.69	3.46	3.98	4.03	4.45	2.02	6.28	5.08	4.59
Eu	1.62	1.94	1.52	1.66	1.52	1.48	1.57	1.70	1.41	1.60	1.66	1.69	1.25	1.44	1.48	1.65	0.80	2.21	1.77	1.67
Gd	4.79	5.83	4.46	5.15	4.31	4.19	4.64	4.93	3.93	4.59	4.67	5.08	3.56	4.15	4.04	4.82	2.45	5.78	5.10	4.54
Tb	0.76	0.96	0.73	0.83	0.70	0.70	0.76	0.80	0.65	0.75	0.75	0.84	0.57	0.65	0.69	0.86	0.43	0.94	0.78	0.73
Dy	4.43	5.60	4.42	5.03	4.15	4.15	4.52	4.65	3.90	4.54	4.50	5.02	3.46	3.96	4.18	5.58	2.67	5.56	4.74	4.25
Ho	0.80	1.03	0.79	0.96	0.76	0.75	0.82	0.85	0.71	0.83	0.85	0.90	0.65	0.72	0.77	1.06	0.50	0.98	0.85	0.77
Er	2.06	2.68	2.09	2.48	1.94	1.99	2.11	2.23	1.91	2.07	2.21	2.34	1.73	1.94	2.02	2.68	1.34	2.37	2.08	1.89
Tm	0.27	0.35	0.28	0.33	0.26	0.26	0.28	0.30	0.25	0.27	0.29	0.31	0.22	0.25	0.26	0.41	0.18	0.31	0.27	0.25
Yb	1.59	2.09	1.69	1.99	1.54	1.61	1.72	1.76	1.56	1.66	1.73	1.86	1.39	1.57	1.63	2.36	1.08	1.86	1.57	1.49
Lu	0.22	0.30	0.25	0.29	0.23	0.22	0.25	0.25	0.21	0.25	0.25	0.26	0.20	0.22	0.24	0.36	0.16	0.25	0.23	0.22
Hf	2.87	3.37	2.83	2.75	2.65	3.20	3.16	3.03	2.37	2.97	2.80	4.87	2.31	2.57	2.59	1.91	1.32	4.17	3.17	3.21
Pb	0.39	0.71	0.41	0.33	0.46	0.48	0.58	0.67	0.42	0.42	0.51	0.78	0.36	0.41	0.45	0.43	0.15	0.80	0.57	0.70
Th	1.68	2.02	1.64	1.66	1.60	1.53	1.82	1.76	1.20	1.70	1.58	1.98	1.21	1.41	1.44	0.64	0.44	2.53	2.09	2.00
U	0.56	0.74	0.34	0.56	0.25	0.87	0.88	0.71	0.33	0.27	0.33	0.46	1.21	0.21	0.24	0.37	0.07	0.30	0.45	0.44
$^{87}Sr/^{86}Sr$ measured	0.705211	0.706115	0.703299	0.706593	0.703291	0.704022	0.705361	0.703560	0.706309	0.703569	0.703584	0.704020	0.703527	0.703517	0.703751	0.704130	0.703777	0.703272	0.703885	0.703293
Error	8	6	8	7	8	21	8	6	9	7	8	14	8	6	9	8	7	9	5	13
$^{87}Sr/^{86}Sr$ (t=56Ma)	0.704614	0.705229	0.703207	0.706166	0.703222	0.703897	0.704983	0.703427	0.705932	0.703437	0.703458	0.703962	0.703441	0.703413	0.703689	0.703824	0.703774	0.703267	0.703808	0.703247
$\delta^{18}O_{SMOW}$	18.0	19.8	8.6	18.9	9.0	15.2	19.2	12.0	22.5	13.0	12.7	20.3	15.5	13.4	19.8	21.0	21.4	10.8	21.7	8.0

Table 1

ODP Leg 197, Hole 1205A						
Core	21R-2	24R-3	34R-1	21R-2	34R-1	34R-4
Interval (cm)	107-112	44-47	106-110	107-112	106-110	94-100
Depth (mbsf)	131.74	151.94	236.06	131.74	236.06	239.89
Piece	13B	8A	19	13B	19	6
Type	Carbonate	Carbonate	Carbonate	Clay	Clay	Clay
Unit	9	10	18B	9	18B	18B
$\delta^{13}C_{PDB}$	-1.55	0.36	-15.27			
$\delta^{18}O_{SMOW}$	30.33	31.60	24.91			
$^{87}Sr/^{86}Sr$	0.707508	0.706642	0.703485	0.706658	0.704390	0.704554
error	10	11	11	10	6	13
Sr (ppm)	163.2	165.3	162.8	44.1	86.2	103.8

Table 2

Unit	Igneous Series	La/Yb group	Alteration zone	Main enrichments	Main depletions	$^{87}Sr/^{86}Sr$ (t=56Ma)	$\delta^{18}O$
7	Upper Igneous Series	High La/Yb	Upper Zone	Fe	Si, Mg, Ca, Na, Sr, Ba	0.704614	18
8A				Fe	Si, Al, Mg, Ca, Na, Sr, Ba	0.703207-0.705229	8.6-19.8
8B				Ca	Si, Al, Fe, Mg, Na, Sr, Ba	0.706166	18.9
9					Si, Sr, Ba	0.703222	9
10				Al, Fe	Si, Mg, Ca, Na, Sr, Ba	0.703427-0.704983	12-19.2
11A				Al, Fe	Si, Mg, Ca, Na, Sr, Ba	0.705932	22.5
11B				Fe	Si, Ca, Na, Sr, Ba	0.703437-0.703458	12.7-13
15B		Low La/Yb	n.d.	Al	Si, Fe, Mg, Ca, Sr, Ba		
18A		High La/Yb	Lower zone	Al, Fe	Si, Mg, Ca, Na, Sr, Ba	0.703962	20.3
18B				Fe	Si, Al, Ca, Na, Sr, Ba	0.703413-0.703689	13.4-19.8
19A	Tholeiitic Unit	n.a.		Al, Fe	Si, Mg, Ca, Na, Sc, Sr, Ba	0.703824	21
19B				Al	Si, Fe, Mg, Sc, Sr, Ba	0.703774	21.4
20	Lower Igneous Series	High La/Yb		Fe	Si, Ca, Na, Sr, Ba		
24A		Low La/Yb		Mg	Si, Al, Fe, Ca, Na, Sr, Ba	*0.703195*	
26A				Mg	Si, Al, Fe, Ca, Na, Sr, Ba		
28A					Si, Al, Fe, Ca, Na, Sr, Ba	*0.703225*	
29B				Sr, Ba	Si, Al, Fe, Ca, Na		

Table 3

	Upper Igneous Serie High La/Yb	σ	Upper Igneous Serie Low La/Yb	σ	Tholeiitic unit	Lower Igneous Serie High La/Yb	σ	Lower Igneous Serie Low La/Yb	σ
La/Yb	8.9	*0.5*	6.8	*0.6*	4.3	12.0	*0.2*	7.1	*0.6*
SiO_2	47.2	*0.5*	47.3	*0.3*	46.2	46.6	*0.8*	47.1	*0.7*
TiO_2	2.5	*0.1*	2.3	*0.3*	1.2	2.8	*0.1*	2.9	*0.3*
Al_2O_3	15.6	*0.4*	15.5	*0.5*	12.1	14.9	*0.3*	15.8	*0.4*
Fe_2O_3	13.6	*1.1*	13.3	*0.7*	13.7	13.8	*0.1*	14.7	*0.7*
MnO	0.2	*0.01*	0.2	*0.1*	0.2	0.2	*0.00*	0.2	*0.0*
MgO	6.5	*0.4*	6.8	*0.4*	16.2	7.3	*0.1*	5.6	*0.5*
CaO	9.2	*0.4*	9.6	*0.3*	7.7	8.8	*0.1*	8.5	*0.2*
Na_2O	3.4	*0.2*	3.3	*0.1*	1.9	3.4	*0.1*	3.5	*0.02*
K_2O	0.8	*0.2*	0.8	*0.3*	0.2	1.1	*0.05*	0.6	*0.5*
P_2O_5	0.5	*0.1*	0.4	*0.05*	0.2	0.7	*0.02*	0.5	*0.1*
LOI	0.5	*0.8*	0.5	*0.4*	0.5	0.5	*0.2*	0.5	*0.5*
Total	100.0	*0.9*	100.0	*0.6*	100.0	100.0	*1.3*	100.0	*1.4*
Sc	26.7	*5.0*	30.5	*2.0*	42.3	26.1	*0.8*	28.6	*2.2*
Rb	13.1	*3.3*	9.6	*2.0*	1.4	17.5	*1.8*	14.7	*2.6*
Sr	436.4	*163.8*	381.4	*61.0*	334.6	639.4	*10.5*	370.5	*32.3*
Y	24.8	*2.0*	24.1	*2.5*	24.2	25.7	*0.1*	29.6	*1.0*
Zr	143.3	*15.1*	126.3	*16.4*	91.1	195.8	*4.7*	190.1	*34.5*
Nb	24.6	*4.6*	20.6	*3.7*	11.3	34.0	*0.3*	26.3	*2.6*
Cs	0.1	*0.04*	0.0	*0.03*	0.0	0.2	*0.1*	0.1	*0.1*
Ba	217.7	*38.7*	172.5	*30.5*	98.7	323.2	*14.5*	228.7	*22.2*
La	16.3	*1.9*	13.2	*2.4*	8.1	22.8	*1.2*	16.5	*2.7*
Ce	36.2	*3.4*	30.1	*5.3*	18.5	49.0	*2.5*	38.1	*7.3*
Pr	4.7	*0.8*	4.2	*0.6*	2.7	6.6	*0.4*	5.4	*1.1*
Nd	20.3	*2.4*	17.6	*2.5*	12.2	26.7	*0.7*	23.4	*4.0*
Sm	4.9	*0.6*	4.5	*0.5*	3.6	6.0	*0.3*	6.0	*1.0*
Eu	1.8	*0.2*	1.6	*0.2*	1.3	2.1	*0.1*	2.1	*0.4*
Gd	5.2	*0.6*	5.0	*0.5*	4.3	6.2	*0.1*	6.3	*0.7*
Tb	0.8	*0.1*	0.8	*0.1*	0.7	0.9	*0.1*	1.0	*0.2*
Dy	4.8	*0.5*	4.6	*0.7*	4.1	5.0	*0.3*	5.7	*1.0*
Ho	0.9	*0.1*	0.9	*0.1*	0.9	1.0	*0.01*	1.1	*0.2*
Er	2.2	*0.2*	2.2	*0.4*	2.1	2.3	*0.2*	2.7	*0.4*
Tm	0.3	*0.03*	0.3	*0.1*	0.3	0.3	*0.0*	0.4	*0.1*
Yb	1.8	*0.2*	1.9	*0.3*	1.9	1.9	*0.1*	2.3	*0.2*
Lu	0.3	*0.03*	0.3	*0.04*	0.3	0.2	*0.04*	0.3	*0.03*
Hf	3.3	*0.4*	3.0	*0.3*	2.5	4.3	*0.2*	4.4	*0.6*
Ta	1.4	*0.3*	1.2	*0.2*	0.8	2.0	*0.1*	1.5	*0.1*
Pb	0.9	*0.3*	0.9	*0.1*	0.5	1.8	*0.01*	1.3	*0.6*
Th	1.7	*0.2*	1.3	*0.2*	0.8	2.4	*0.1*	1.6	*0.1*
U	0.4	*0.1*	0.3	*0.1*	0.2	0.7	*0.01*	0.5	*0.04*

Table 4

Rock type	Breccia	2%<LOI<5% (slightly altered)	5%<LOI<10% (moderately altered)	10%<LOI<15% (highly altered)	LOI>15% (intensely altered)	Soil	Recovered proportions	Model A	Model B	Model C
n	1	7	4	5	3	4				
SiO_2	-21.8	-2.4	-4.4	-6.1	-12.1	-18.5	-4.5	-6.1	-7.2	-7.7
TiO_2	-0.6	-0.2	0.2	-0.1	0.1	0.2	0.02	0.02	-0.02	-0.03
Al_2O_3	-5.6	-1.0	0.2	-0.4	-0.1	1.6	-0.3	-0.4	-0.6	-0.6
Fe_2O_3	-2.4	-0.5	1.1	1.6	3.8	1.7	0.6	0.7	0.7	0.6
MnO	-0.01	-0.01	0.01	0.00	0.00	-0.08	0.00	0.00	0.00	-0.01
MgO	-4.0	0.0	-2.3	-1.0	-3.7	-7.7	-1.5	-2.0	-2.2	-2.3
CaO	5.9	-0.7	-2.4	-3.9	-6.3	-7.5	-2.0	-2.3	-2.2	-2.1
Na_2O	-2.2	-0.3	-0.5	-0.7	-1.5	-1.9	-0.5	-0.7	-0.8	-0.8
K_2O	0.1	-0.1	0.1	0.0	0.2	-0.1	0.02	0.03	0.04	0.03
P_2O_5	0.0	-0.1	-0.1	-0.1	0.0	-0.2	-0.1	-0.1	-0.1	-0.1
Sc	-13.0	-2.2	-9.4	-10.3	-7.5	-14.1	-7.2	-8.3	-8.3	-8.5
Rb	-1.1	-3.3	-1.0	-5.7	0.2	-2.6	-2.5	-2.5	-2.4	-2.4
Sr	-371.6	-89.2	-161.7	-314.1	-334.0	-357.2	-166.6	-197.9	-213.4	-215.6
Y	1.7	-1.2	-2.7	-4.8	-1.6	-7.0	-2.5	-2.8	-2.6	-2.6
Zr	-33.5	-23.6	-22.2	-35.4	-19.0	-22.7	-24.7	-25.5	-25.4	-25.5
Cs	0.00	-0.04	0.02	0.03	0.14	0.10	0.00	0.01	0.02	0.02
Nb	-9.2	-4.5	-4.0	-8.3	-5.7	-6.5	-4.9	-5.3	-5.5	-5.6
Ba	-145.1	-38.3	-41.1	-98.8	-114.4	-133.9	-51.7	-63.0	-70.7	-72.4
La	-1.1	-0.9	-0.2	-2.1	-0.2	-1.7	-0.8	-0.9	-0.9	-0.9
Ce	-2.9	-1.4	0.0	-3.7	0.0	-1.8	-1.0	-1.3	-1.3	-1.4
Pr	-0.7	-0.6	-0.4	-1.3	-0.7	-1.1	-0.6	-0.7	-0.7	-0.7
Nd	-1.9	-1.7	-1.0	-3.9	-1.1	-3.4	-1.7	-1.9	-1.9	-1.9
Sm	-0.5	-0.5	-0.4	-0.9	-0.3	-0.7	-0.5	-0.6	-0.5	-0.6
Eu	-0.2	-0.1	-0.1	-0.3	-0.1	-0.2	-0.1	-0.2	-0.2	-0.2
Gd	-0.5	-0.5	-0.4	-1.1	-0.5	-0.9	-0.5	-0.6	-0.6	-0.6
Tb	0.0	0.0	0.0	-0.1	0.0	-0.1	-0.1	-0.1	-0.1	-0.1
Dy	-0.1	-0.3	-0.3	-0.6	-0.1	-0.4	-0.3	-0.3	-0.3	-0.3
Ho	0.0	-0.1	-0.1	-0.2	-0.1	-0.2	-0.1	-0.1	-0.1	-0.1
Er	0.0	-0.1	-0.1	-0.3	0.0	-0.2	-0.1	-0.1	-0.1	-0.1
Tm	0.01	-0.02	-0.02	-0.03	0.00	-0.02	-0.02	-0.02	-0.02	-0.02
Yb	0.0	-0.2	-0.1	-0.3	0.0	-0.2	-0.2	-0.2	-0.2	-0.2
Lu	0.01	-0.02	-0.02	-0.03	0.00	-0.03	-0.02	-0.02	-0.02	-0.02
Hf	-0.8	-0.5	-0.4	-0.7	-0.3	-0.5	-0.5	-0.5	-0.5	-0.5
Pb	-0.6	-0.1	-0.3	-0.7	-0.4	-0.4	-0.3	-0.3	-0.3	-0.3
Th	-0.2	-0.2	0.0	-0.2	0.0	-0.2	-0.1	-0.1	-0.1	-0.2
U	0.1	0.1	0.0	0.2	0.2	0.1	0.1	0.1	0.1	0.1

Table 5

	Breccia	Slightly altered basalt	Moderately altered basalt	Highly altered basalt	Completely altered basalt	Soil	Total
Recovered proportions total length (cm	255	5960	8925	2648	90	250	18128
Recovered proportions %	1.4	32.9	49.2	14.6	0.5	1.4	100
Model A total length (cm)	1275	6622	12750	5296	450	1786	28179
Model A %	4.5	23.5	45.3	18.8	1.6	6.3	100
Model B total length (cm)	2295	6980	10149	4688	2130	2086	28330
Model B %	8.1	24.6	35.8	16.6	7.5	7.4	100
Model C total length (cm)	2833	7083	9916	4250	1416.5	2833	28330
Model C %	10	25	35	15	5	10	100

Table 6

	Nintoku		Hole 504B, LT alteration		Site 417/418			Juan de Fuca Ridge	Eastern flank East Pacific Rise	
	Min	Max	(a)	(b)	(b)	(c)	(a), (d)	(a), (e)	(f)	
Si	3.2	20	140	-31	-71	-71		1.8 (a)		$x10^{10}$ mol/yr
Ca	1.6	11	21.7	2.9	-140 to 140	-140	120 (d)	470 (a)		$x10^{10}$ mol/yr
Mg	1.6	11	-34.5	-30.8	-26	17	-14 (d)	-540 (a)		$x10^{10}$ mol/yr
K	-0.011	-0.11	-9.8	-6.5	-40 to -49	-21	-41 (d)	-33 (a)	-0.12	$x10^{10}$ mol/yr
Fe	-0.16	-1.7		-18	-1	0.39		0 (e)		$x10^{10}$ mol/yr
Al	-0.5	0.6				-69				$x10^{10}$ mol/yr
Na	0.35	2.2				-8.7	-22 (d)	-62 (e)		$x10^{10}$ mol/yr
Cs	-0.00007	0.0073	-1.5				-6.5 (a)		-0.05	$x10^{6}$ mol/yr
Rb	0.0057	0.52	-81		-38		-490 (a)	-26 (a)	-2.2	$x10^{6}$ mol/yr
U	-0.001	-0.0078	-0.9		-4		-9.7 (a)	-1.4 (a)	-0.033	$x10^{6}$ mol/yr
Sr	8.3	42						250 (e)		$x10^{6}$ mol/yr
Ba	1.6	8.6							-13	$x10^{6}$ mol/yr

Table 7

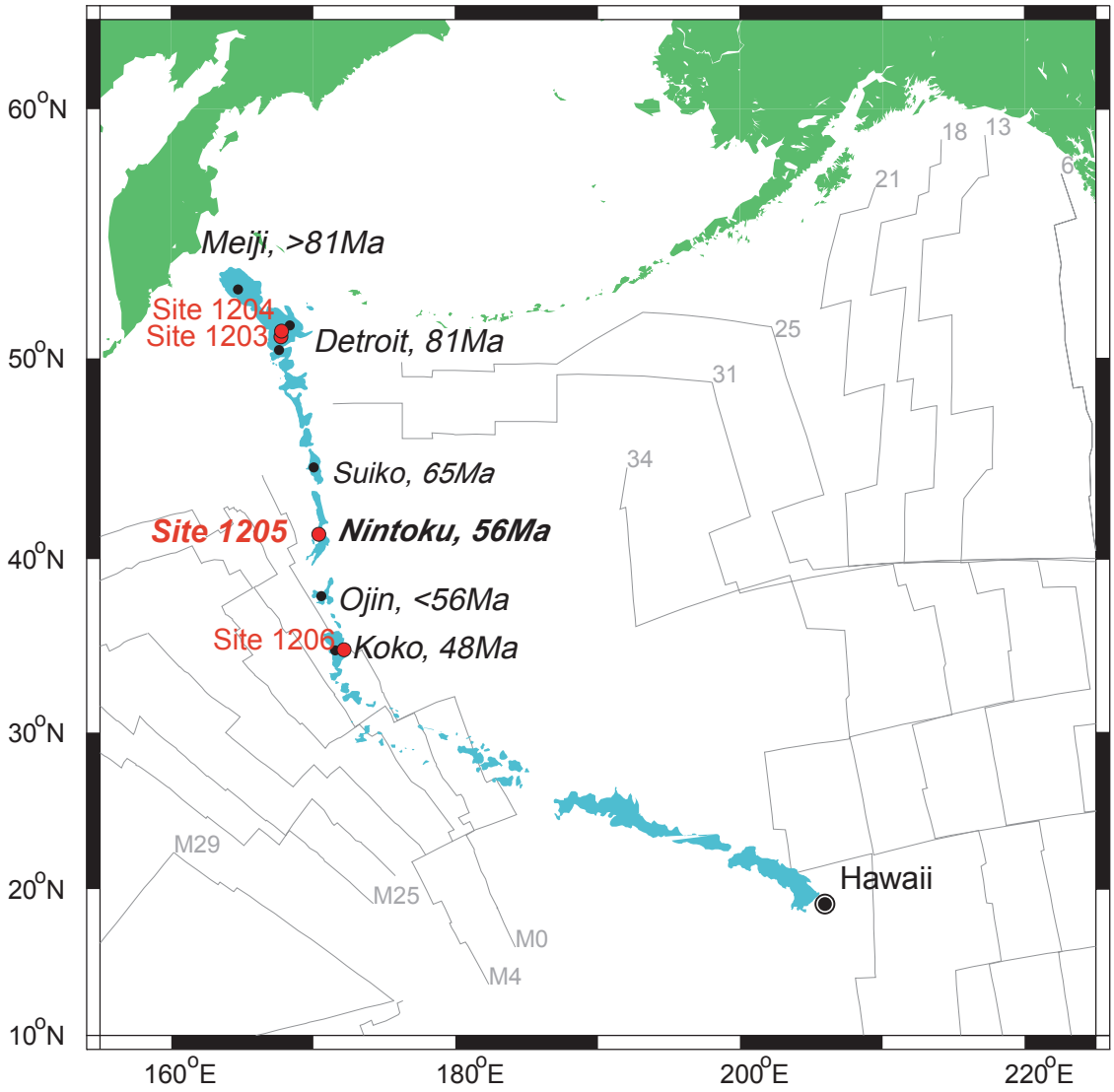
60°N
50°N
40°N
30°N
20°N
10°N
160°E
180°E
200°E
220°E
Meiji, >81Ma
Site 1204
Site 1203
Detroit, 81Ma
Suiko, 65Ma
Site 1205
Nintoku, 56Ma
Ojin, <56Ma
Site 1206
Koko, 48Ma
Hawaii
18
13
6
21
25
31
34
M29
M25
M0
M4

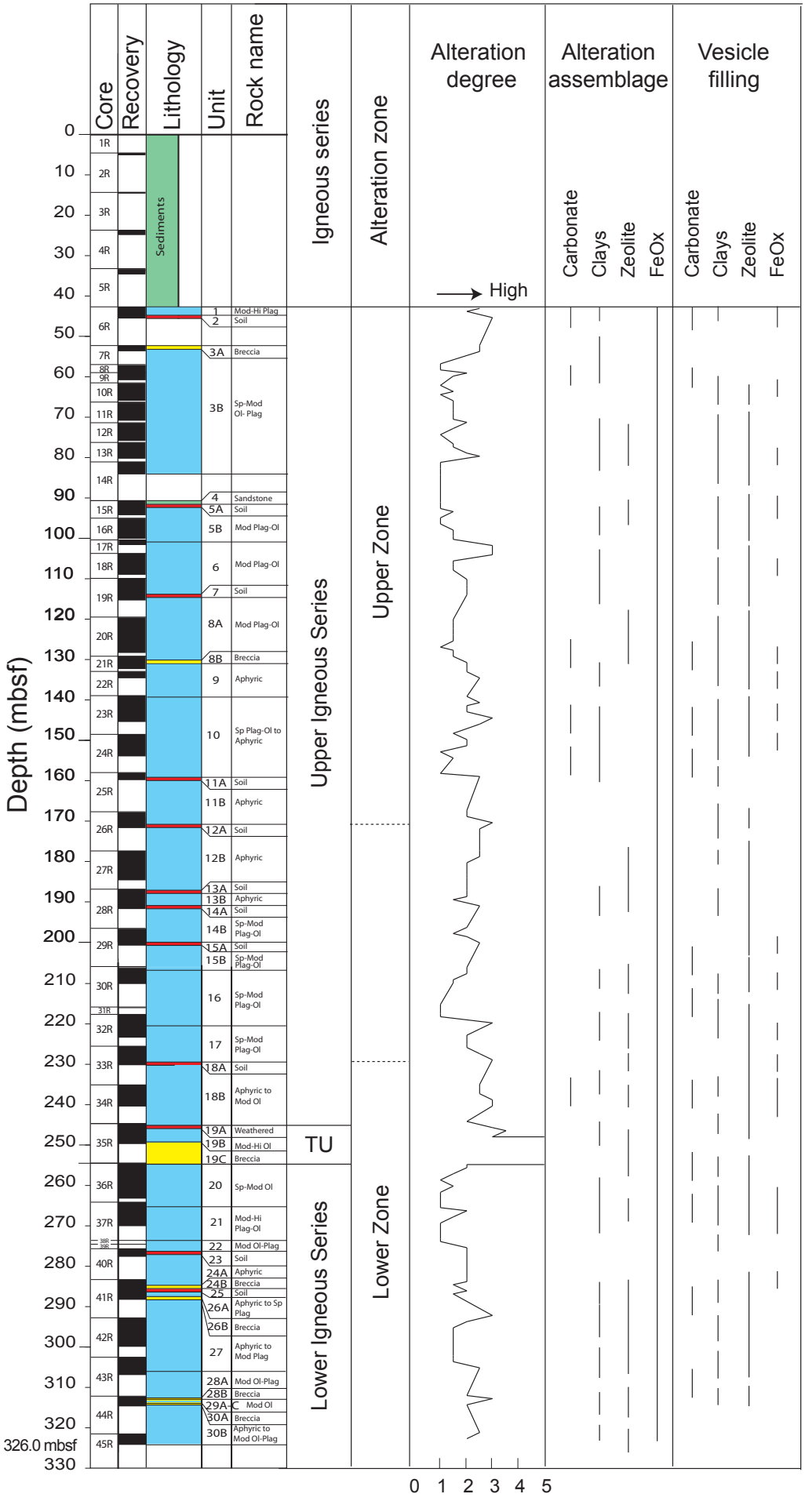
Depth (mbsf)
Core
Recovery
Lithology
Unit
Rock name
Igneous series
Alteration zone
Alteration degree
Alteration assemblage
Vesicle filling
Sediments
Mod-Hi Plag
Soil
Breccia
Sp-Mod Ol- Plag
Sandstone
Mod Plag-Ol
Aphyric
Sp Plag-Ol to Aphyric
Weathered
Mod-Hi Ol
Sp-Mod Ol
Mod-Hi Plag-Ol
Mod Ol-Plag
Aphyric to Sp Plag
Aphyric to Mod Plag
Mod Ol
Aphyric to Mod Ol-Plag
Upper Igneous Series
Lower Igneous Series
TU
Upper Zone
Lower Zone
High
Carbonate
Clays
Zeolite
FeOx
TD 326.0 mbsf
0 1 2 3 4 5

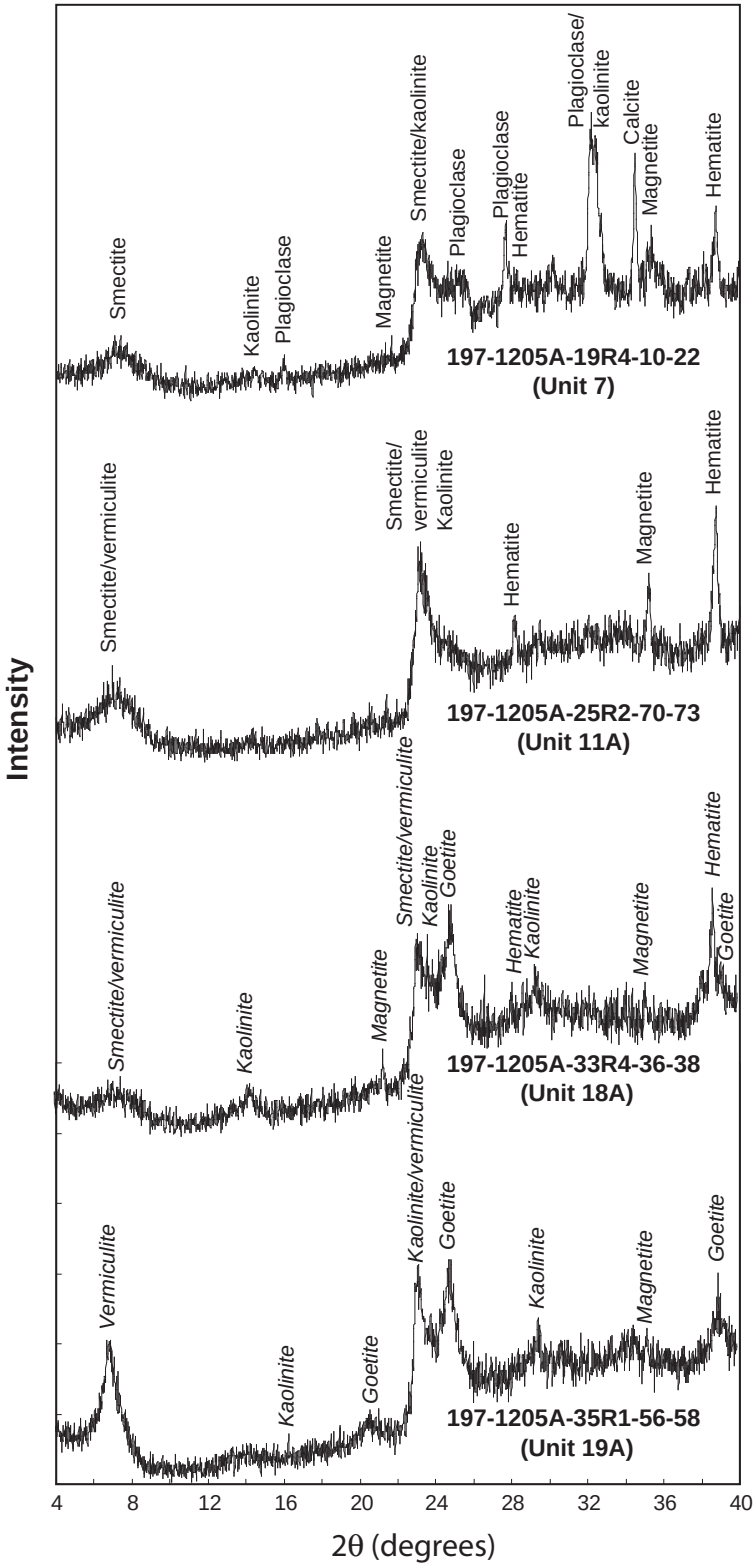
Intensity
Smectite
Kaolinite
Plagioclase
Magnetite
Smectite/kaolinite
Plagioclase
Plagioclase
Hematite
Plagioclase/
kaolinite
Calcite
Magnetite
Hematite
197-1205A-19R4-10-22
(Unit 7)
Smectite/vermiculite
Smectite/
vermiculite
Kaolinite
Hematite
Magnetite
Hematite
197-1205A-25R2-70-73
(Unit 11A)
Smectite/vermiculite
Kaolinite
Magnetite
Smectite/vermiculite
Kaolinite
Goetite
Hematite
Kaolinite
Magnetite
Hematite
Goetite
197-1205A-33R4-36-38
(Unit 18A)
Vermiculite
Kaolinite
Goetite
Kaolinite/vermiculite
Goetite
Kaolinite
Magnetite
Goetite
197-1205A-35R1-56-58
(Unit 19A)
4
8
12
16
20
24
28
32
36
40
2θ (degrees)

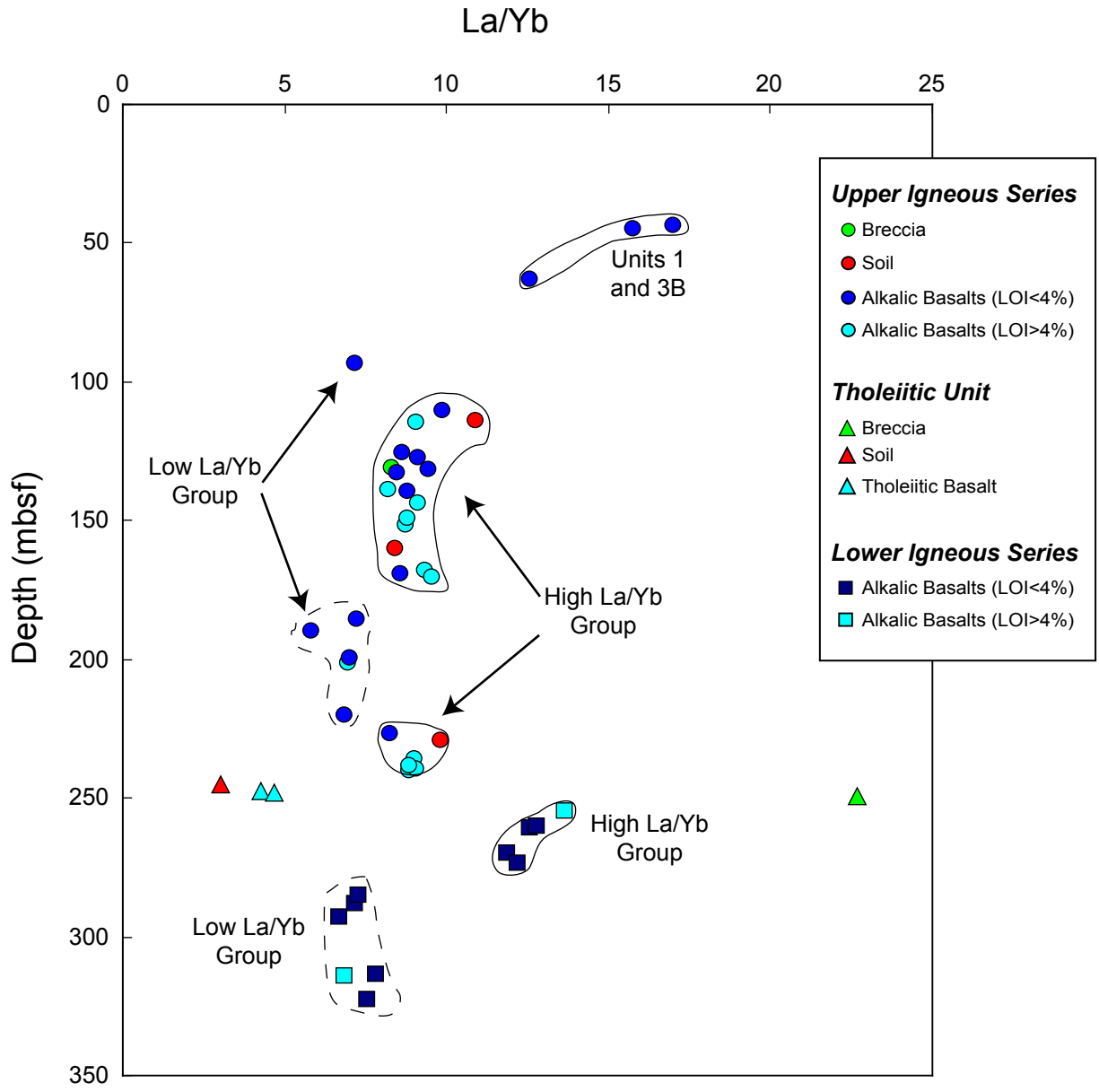
La/Yb
0
5
10
15
20
25
0
50
100
150
200
250
300
350
Depth (mbsf)
Units 1
and 3B
Low La/Yb
Group
High La/Yb
Group
High La/Yb
Group
Low La/Yb
Group
Upper Igneous Series
Breccia
Soil
Alkalic Basalts (LOI<4%)
Alkalic Basalts (LOI>4%)
Tholeiitic Unit
Breccia
Soil
Tholeiitic Basalt
Lower Igneous Series
Alkalic Basalts (LOI<4%)
Alkalic Basalts (LOI>4%)

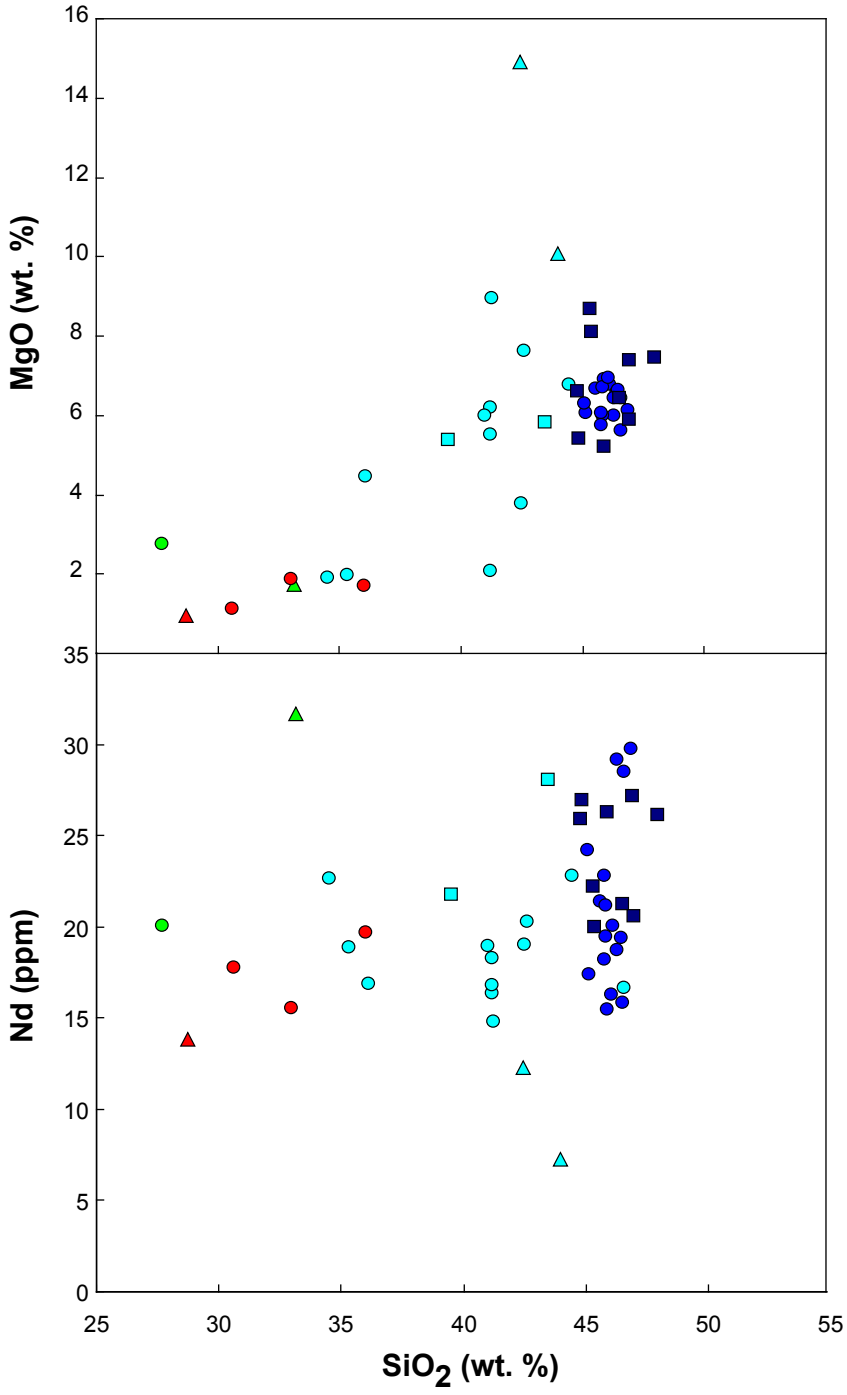
MgO (wt. %)
16
14
12
10
8
6
4
2
Nd (ppm)
35
30
25
20
15
10
5
0
25
30
35
40
45
50
55
SiO2 (wt. %)

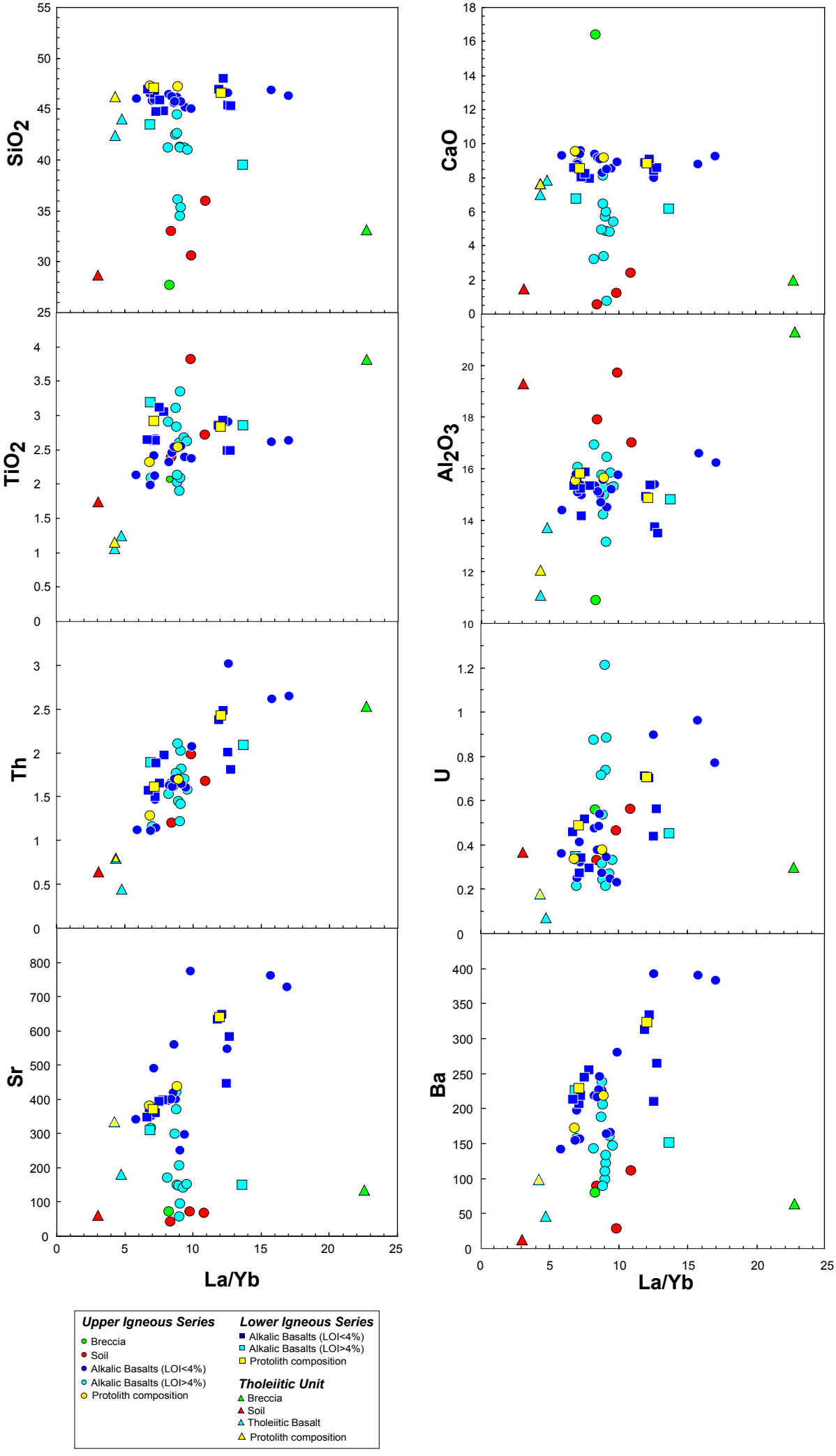
SiO2
TiO2
Th
Sr
CaO
Al2O3
U
Ba
La/Yb
La/Yb
Upper Igneous Series
Breccia
Soil
Alkalic Basalts (LOI<4%)
Alkalic Basalts (LOI>4%)
Protolith composition
Lower Igneous Series
Alkalic Basalts (LOI<4%)
Alkalic Basalts (LOI>4%)
Protolith composition
Tholeiitic Unit
Breccia
Soil
Tholeiitic Basalt
Protolith composition

Gains
10
1
0.1
0.01
TiO2
Al2O3
Fe2O3
MgO
CaO
Na2O
K2O
Rb
Y
La
Nd
Yb
Th
U
Losses
1000
100
10
1
SiO2
Al2O3
Fe2O3
MgO
CaO
Na2O
Sc
Rb
Sr
Y
Ba
La
Nd
Losses
1
0.1
0.01
TiO2
Al2O3
Fe2O3
MgO
CaO
Na2O
K2O
Y
La
Nd
Yb
Pb
Th
U
Upper Igneous Series, High La/Yb,
Unit 7, Soil
Unit 8A
Unit 8B, Breccia
Unit 9
Unit 10
Unit 11A, Soil
Unit 11B
Unit 18A, Soil
Unit 18B

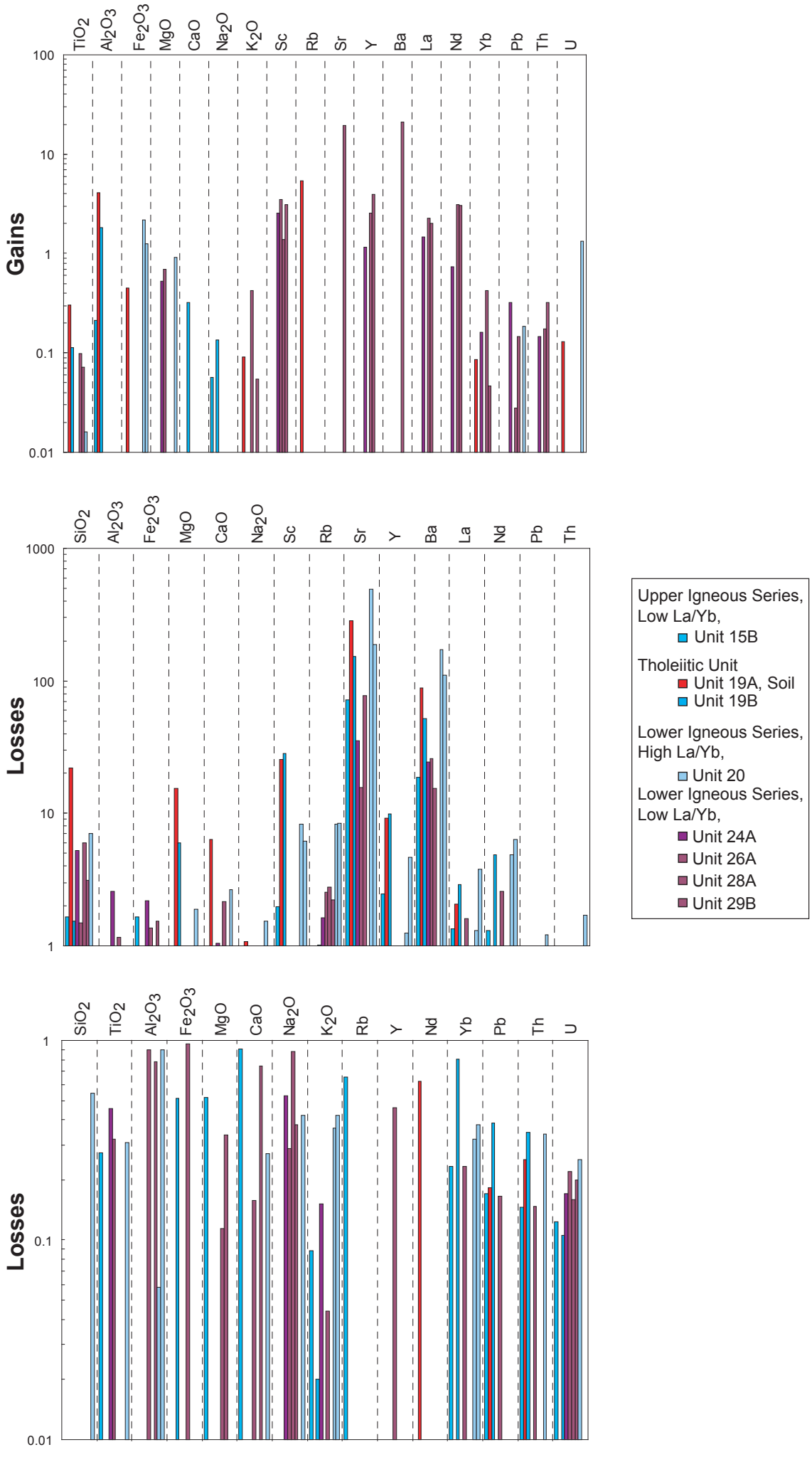
Gains
TiO2
Al2O3
Fe2O3
MgO
CaO
Na2O
K2O
Sc
Rb
Sr
Y
Ba
La
Nd
Yb
Pb
Th
U
100
10
1
0.1
0.01
Losses
SiO2
Al2O3
Fe2O3
MgO
CaO
Na2O
Sc
Rb
Sr
Y
Ba
La
Nd
Pb
Th
1000
100
10
1
Losses
SiO2
TiO2
Al2O3
Fe2O3
MgO
CaO
Na2O
K2O
Rb
Y
Nd
Yb
Pb
Th
U
1
0.1
0.01
Upper Igneous Series, Low La/Yb,
Unit 15B
Tholeiitic Unit
Unit 19A, Soil
Unit 19B
Lower Igneous Series, High La/Yb,
Unit 20
Lower Igneous Series, Low La/Yb,
Unit 24A
Unit 26A
Unit 28A
Unit 29B

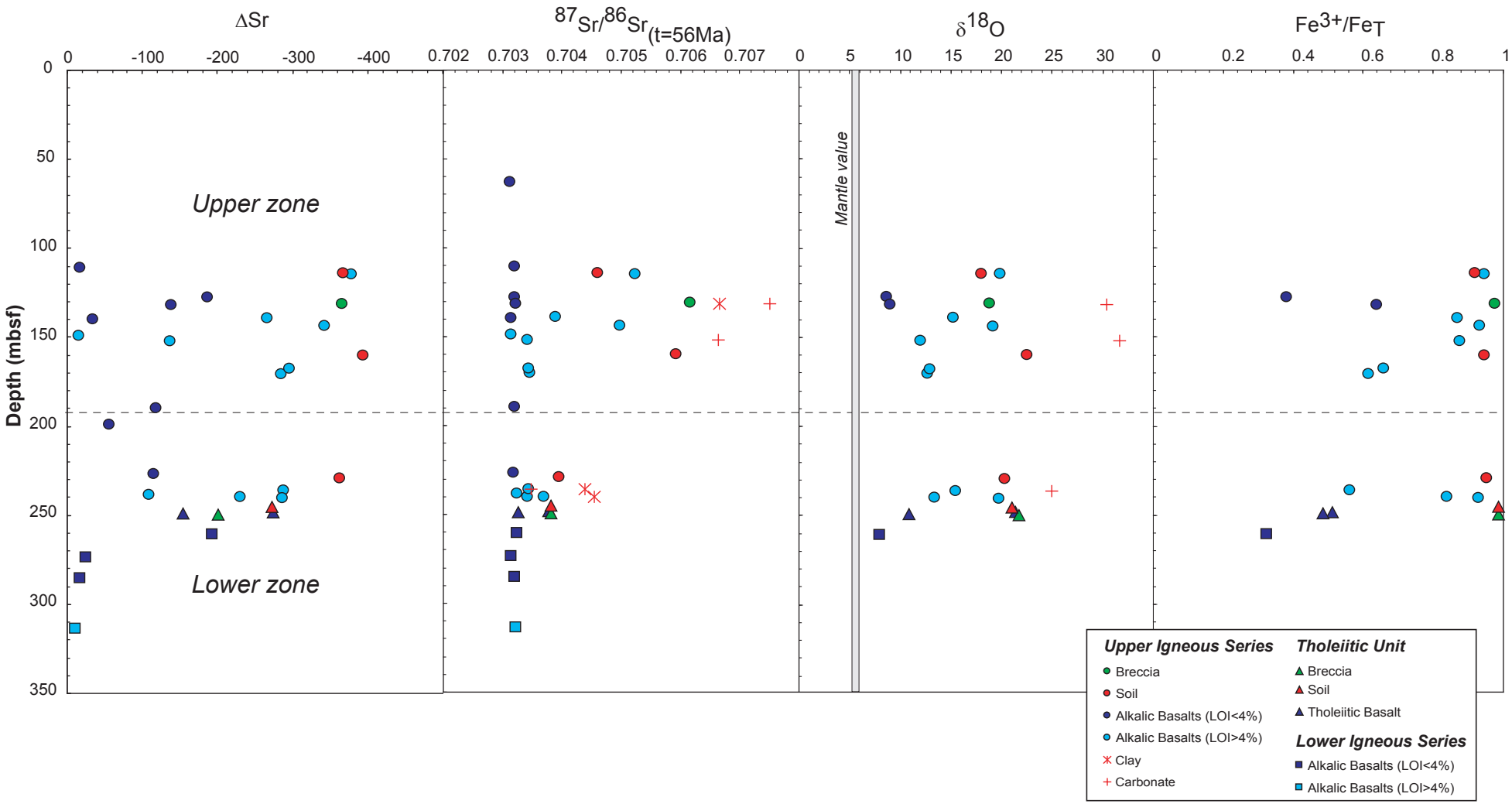
ΔSr
87Sr/86Sr(t=56Ma)
δ18O
Fe3+/FeT
Depth (mbsf)
Upper zone
Lower zone
Mantle value
Upper Igneous Series
Breccia
Soil
Alkalic Basalts (LOI<4%)
Alkalic Basalts (LOI>4%)
Clay
Carbonate
Tholeiitic Unit
Breccia
Soil
Tholeiitic Basalt
Lower Igneous Series
Alkalic Basalts (LOI<4%)
Alkalic Basalts (LOI>4%)

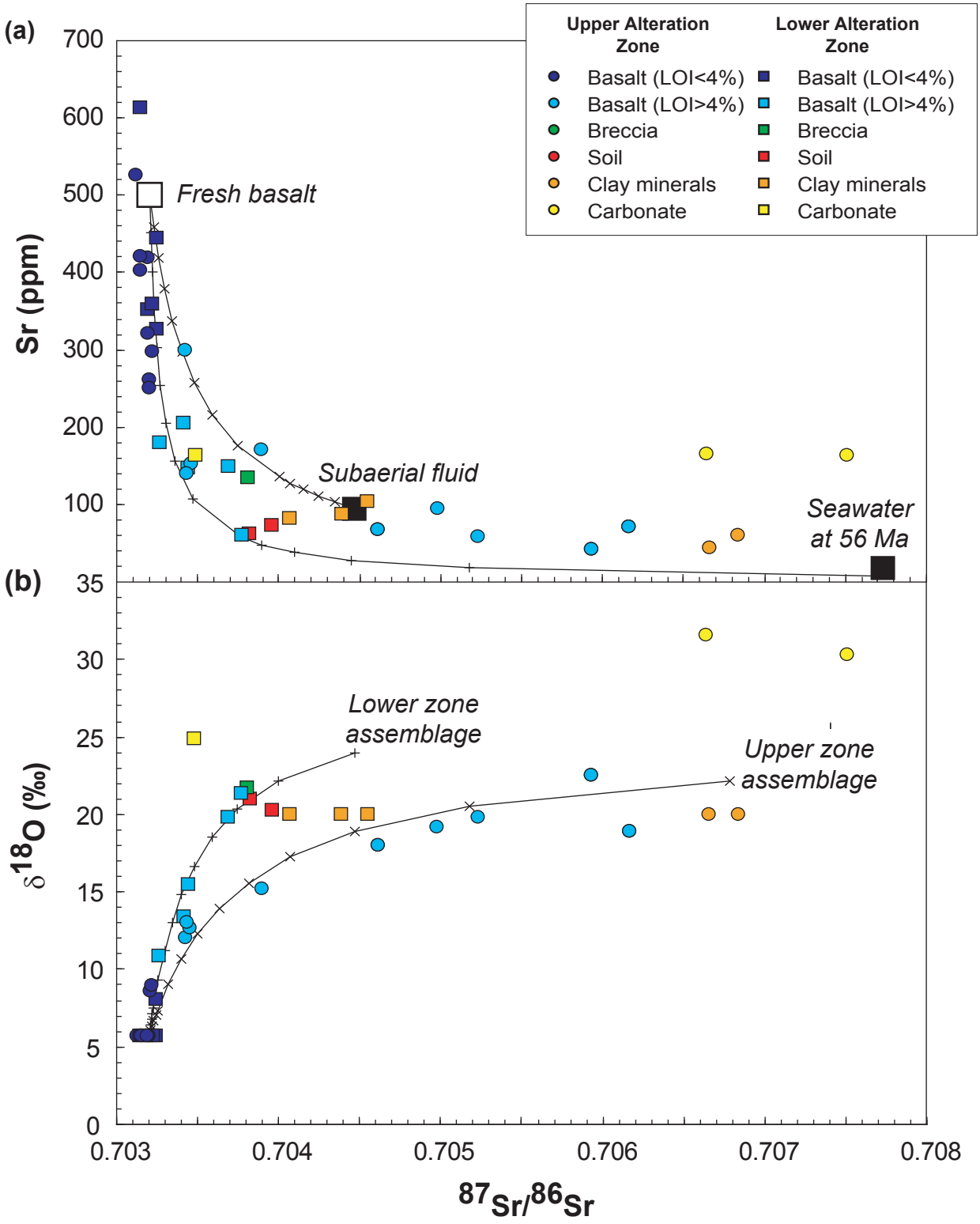
(a)
(b)
Upper Alteration Zone
Lower Alteration Zone
Basalt (LOI<4%)
Basalt (LOI>4%)
Breccia
Soil
Clay minerals
Carbonate
Fresh basalt
Subaerial fluid
Seawater at 56 Ma
Lower zone assemblage
Upper zone assemblage
Sr (ppm)
δ18O (‰)
87Sr/86Sr
0
5
10
15
20
25
30
35
100
200
300
400
500
600
700
0.703
0.704
0.705
0.706
0.707
0.708

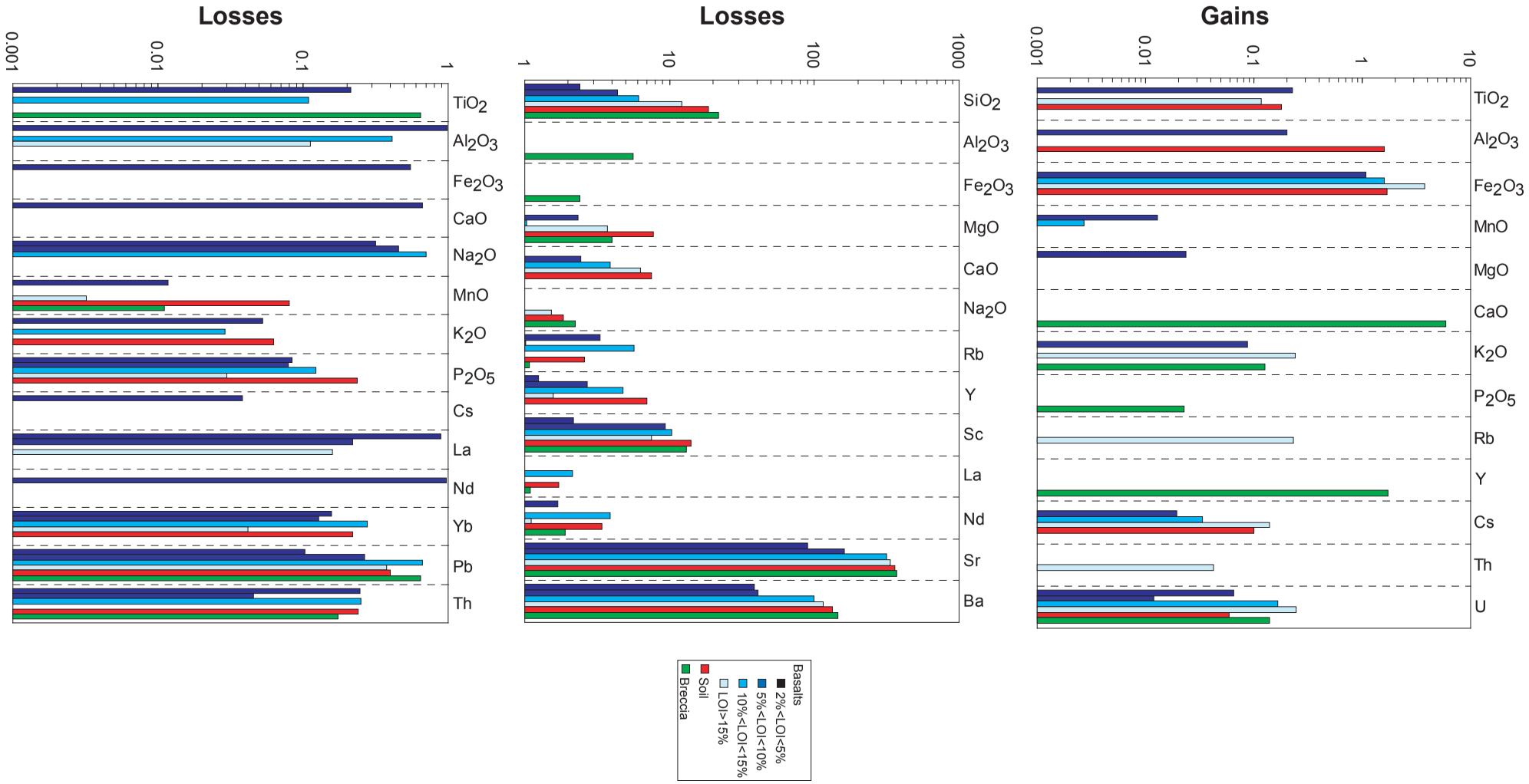
Losses
0.001
0.01
0.1
1
TiO2
Al2O3
Fe2O3
CaO
Na2O
MnO
K2O
P2O5
Cs
La
Nd
Yb
Pb
Th
Losses
1
10
100
1000
SiO2
Al2O3
Fe2O3
MgO
CaO
Na2O
Rb
Y
Sc
La
Nd
Sr
Ba
Gains
0.001
0.01
0.1
1
10
TiO2
Al2O3
Fe2O3
MnO
MgO
CaO
K2O
P2O5
Rb
Y
Cs
Th
U
Basalts
2%<LOI<5%
5%<LOI<10%
10%<LOI<15%
LOI>15%
Soil
Breccia

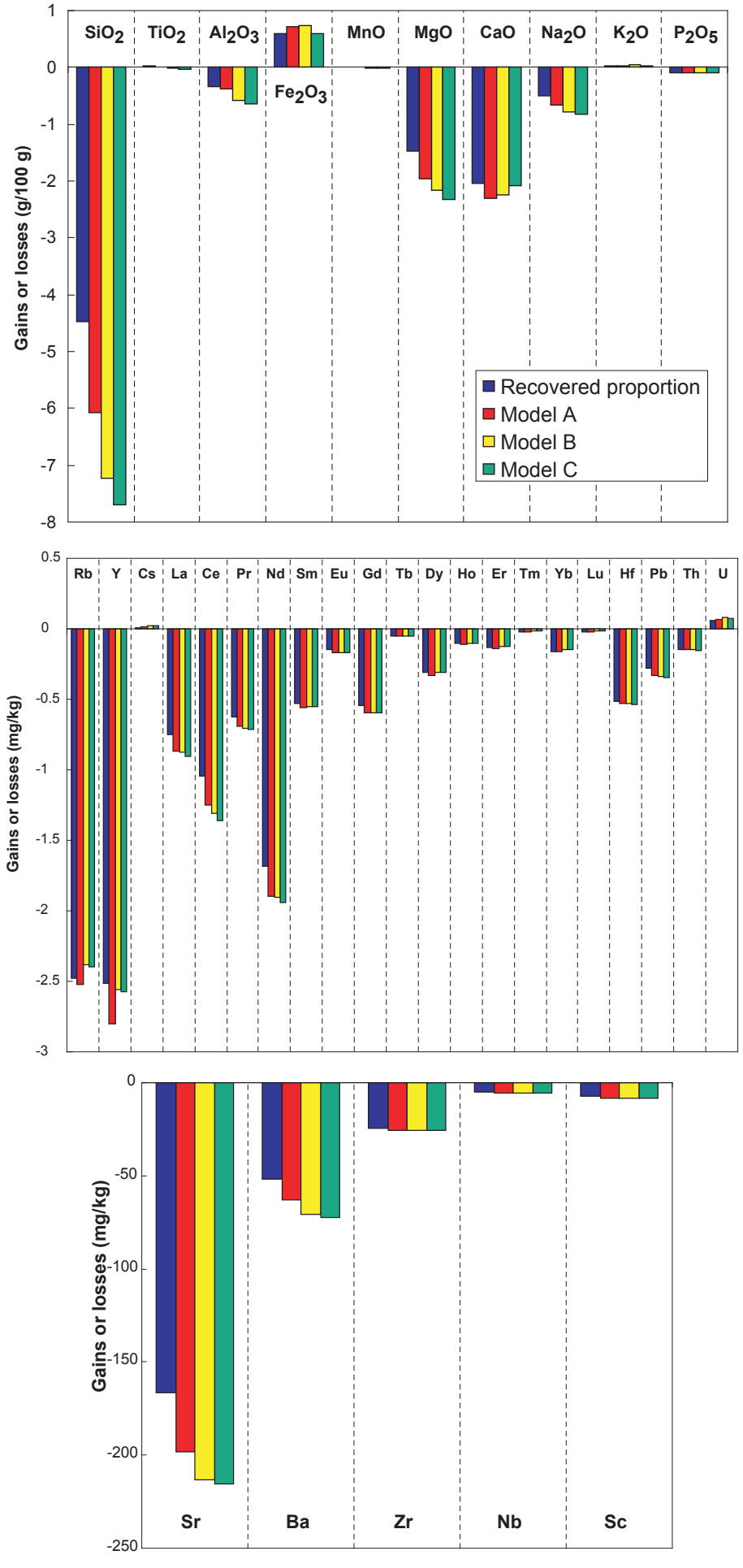
Gains or losses (g/100 g)
1
0
-1
-2
-3
-4
-5
-6
-7
-8
SiO2
TiO2
Al2O3
Fe2O3
MnO
MgO
CaO
Na2O
K2O
P2O5
Recovered proportion
Model A
Model B
Model C
Gains or losses (mg/kg)
0.5
0
-0.5
-1
-1.5
-2
-2.5
-3
Rb
Y
Cs
La
Ce
Pr
Nd
Sm
Eu
Gd
Tb
Dy
Ho
Er
Tm
Yb
Lu
Hf
Pb
Th
U
Gains or losses (mg/kg)
0
-50
-100
-150
-200
-250
Sr
Ba
Zr
Nb
Sc

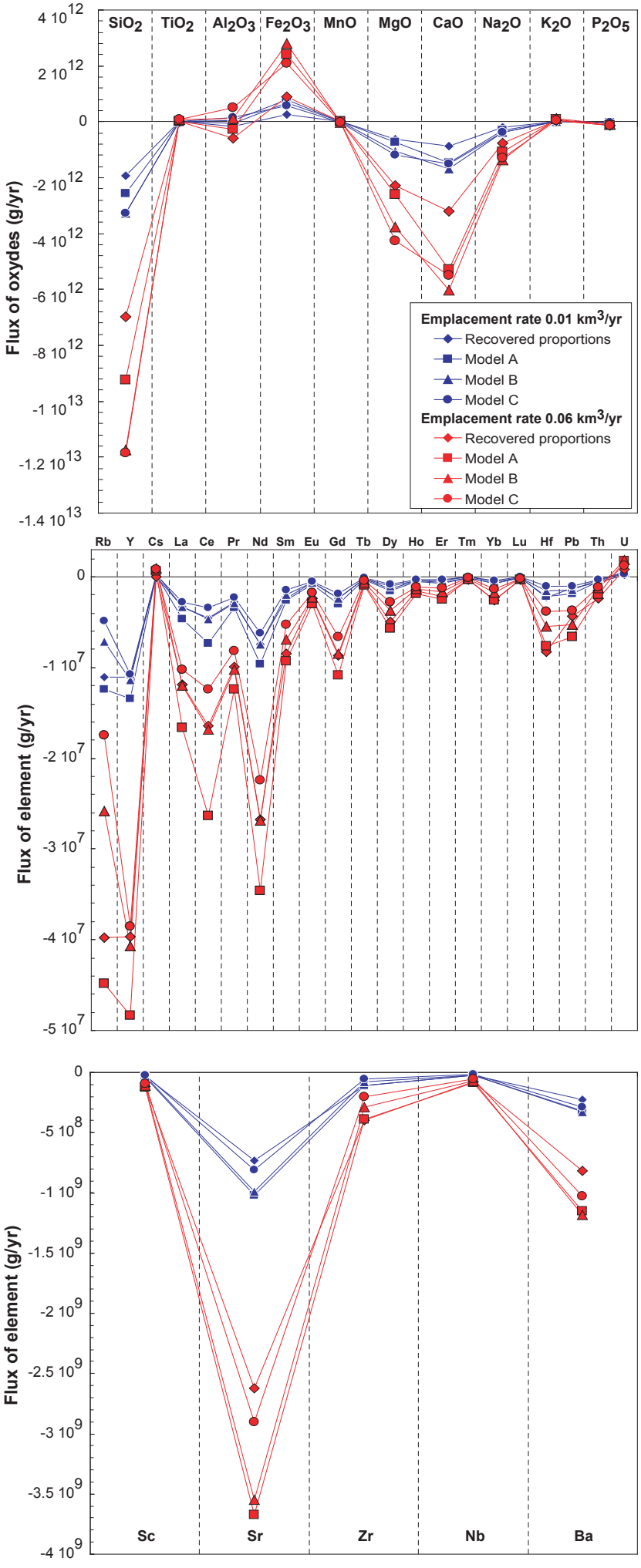
SiO2
TiO2
Al2O3
Fe2O3
MnO
MgO
CaO
Na2O
K2O
P2O5
Flux of oxydes (g/yr)
4 10^12
2 10^12
0
-2 10^12
-4 10^12
-6 10^12
-8 10^12
-1 10^13
-1.2 10^13
-1.4 10^13
Emplacement rate 0.01 km3/yr
Recovered proportions
Model A
Model B
Model C
Emplacement rate 0.06 km3/yr
Recovered proportions
Model A
Model B
Model C
Rb Y Cs La Ce Pr Nd Sm Eu Gd Tb Dy Ho Er Tm Yb Lu Hf Pb Th U
Flux of element (g/yr)
0
-1 10^7
-2 10^7
-3 10^7
-4 10^7
-5 10^7
Flux of element (g/yr)
0
-5 10^8
-1 10^9
-1.5 10^9
-2 10^9
-2.5 10^9
-3 10^9
-3.5 10^9
-4 10^9
Sc
Sr
Zr
Nb
Ba